
Constitutive modelling of passive myocardium: a structurally based framework for material characterization

Gerhard A. Holzapfel and Ray W. Ogden

Phil. Trans. R. Soc. A 2009 **367**, doi: 10.1098/rsta.2009.0091, published 3 August 2009

References

This article cites 35 articles, 10 of which can be accessed free
<http://rsta.royalsocietypublishing.org/content/367/1902/3445.full.html#ref-list-1>

Article cited in:

<http://rsta.royalsocietypublishing.org/content/367/1902/3445.full.html#related-urls>

Subject collections

Articles on similar topics can be found in the following collections

[biomedical engineering](#) (145 articles)

Email alerting service

Receive free email alerts when new articles cite this article - sign up in the box at the top right-hand corner of the article or click [here](#)

Constitutive modelling of passive myocardium: a structurally based framework for material characterization

BY GERHARD A. HOLZAPFEL^{1,2,*} AND RAY W. OGDEN³

¹*Department of Solid Mechanics, School of Engineering Sciences, Royal Institute of Technology (KTH), Osquars Backe 1, 100 44 Stockholm, Sweden*
²*Institute of Biomechanics, Center of Biomedical Engineering, Graz University of Technology, Kronesgasse 5-I, 8010 Graz, Austria*
³*Department of Mathematics, University of Glasgow, University Gardens, Glasgow G12 8QW, UK*

In this paper, we first of all review the morphology and structure of the myocardium and discuss the main features of the mechanical response of passive myocardium tissue, which is an orthotropic material. Locally within the architecture of the myocardium three mutually orthogonal directions can be identified, forming planes with distinct material responses. We treat the left ventricular myocardium as a non-homogeneous, thick-walled, nonlinearly elastic and incompressible material and develop a general theoretical framework based on invariants associated with the three directions. Within this framework we review existing constitutive models and then develop a structurally based model that accounts for the muscle fibre direction and the myocyte sheet structure. The model is applied to simple shear and biaxial deformations and a specific form fitted to the existing (and somewhat limited) experimental data, emphasizing the orthotropy and the limitations of biaxial tests. The need for additional data is highlighted. A brief discussion of issues of convexity of the model and related matters concludes the paper.

Keywords: myocardium; constitutive modelling; orthotropy; muscle fibres; myocyte sheet structure

1. Introduction

Of central importance for the better understanding of the fundamental mechanisms underlying ventricular mechanics are: (i) realistic descriptions of the three-dimensional geometry and structure of the myocardium, (ii) continuum balance laws and boundary conditions and, most importantly, (iii) constitutive equations that characterize the material properties of the myocardium, including their spatial and temporal variations, together with statistical parameter estimation and optimization, and validation. To characterize the material properties, it is essential to have available comprehensive force–deformation data from a range of different deformation modes. In particular, a combination of

*Author for correspondence (holzapfel@tugraz.at).

biaxial test data with different loading protocols and shear test data at different specimen orientations is required to capture adequately the direction-dependent nonlinear material response.

The purpose of this paper is to develop a general theoretical framework within the context of nonlinear elasticity theory that takes account of the structural features of the myocardium and its orthotropic properties. Within that framework, we then consider specific models for the myocardium to characterize its passive mechanical response. There are several models of the elasticity of the myocardium available in the literature, including isotropic models (e.g. [Demiray 1976](#)), transversely isotropic models (e.g. [Humphrey & Yin 1987](#); [Humphrey *et al.* 1990](#); [Guccione *et al.* 1991](#); [Costa *et al.* 1996](#)) and, more recently, orthotropic models (e.g. [Hunter *et al.* 1997](#); [Costa *et al.* 2001](#); [Schmid *et al.* 2006](#)). We review these and several others briefly in §4. For a recent account of modelling aspects of the mechanics of the heart and arteries, we refer to the edited volume by [Holzapfel & Ogden \(2009\)](#).

One problem in developing an adequate constitutive model is the shortage of experimental data suitable for detailed parameter estimation in specific functional forms. Early contributions to gathering such data are contained in the work of [Demer & Yin \(1983\)](#) and [Yin *et al.* \(1987\)](#) in which data from biaxial tests were obtained. However, as we shall emphasize later, data from biaxial tests alone are not enough to characterize the passive response of myocardium because such data suggest that the material is transversely isotropic. That this is not the case has been demonstrated clearly in the more recent work by [Dokos *et al.* \(2002\)](#), which, on the basis of shear tests conducted on cube-shaped specimens from different orientations within the myocardium, highlighted the orthotropic behaviour of the material. It remains the case, however, that there is a need for more comprehensive sets of data to be obtained.

In §2, we outline the key features of the morphology and structure of the myocardium and then describe the passive mechanical response of myocardial tissue on the basis of the available biaxial and shear test data. Against this background, we then construct, in §3, a general framework for the elastic strain-energy function based on the use of invariants that are related to the myocardium structure. This framework embraces most, if not all, of the elasticity-based constitutive models for the passive myocardium that have appeared in the literature to date. Next, in §4, as mentioned above, we review the existing models within this framework. In §5, guided by data from shear and biaxial tests, we develop an appropriately specialized form of the general strain-energy function from §3. This is then specialized further by the introduction of specific functional forms for the dependence of the energy function on the restricted set of invariants that it includes. The model so constructed is then evaluated against the considered shear and biaxial data, and values of the material constants it contains are obtained by curve fitting. The general features of the shear data of [Dokos *et al.* \(2002\)](#) are reproduced by using six material constants, whereas eight constants are needed to recover finer details of the data. To fit the biaxial data, a transversely isotropic specialization of the model suffices to give a reasonable fit to the data of [Yin *et al.* \(1987\)](#) and only four material constants are needed. This highlights the point already alluded to that biaxial tests alone are not sufficient to extract the orthotropic nature of the tissue and should not therefore be used in isolation.

In §6, we examine the form of strain-energy function constructed with reference to inequalities that ensure ‘physically reasonable response’, including the monotonicity of the stress deformation behaviour in uniaxial tests and notions of convexity and strong ellipticity in three dimensions. These all require, in particular, that the material constants included in various terms contributing to the strain energy are positive, which is consistent with the values obtained in fitting the data. Finally, §7 is devoted to a concluding discussion.

2. Morphology, structure and typical mechanical behaviour of the passive myocardium

(a) Morphology and structure

The human heart consists of four chambers, namely the right and left *atria*, which receive blood from the body, and the left and right *ventricles*, which pump blood around the body. For a detailed description of the individual functionalities of these four chambers, see [Katz \(1977\)](#). There is still an ongoing debate concerning the structure of the heart ([Gilbert *et al.* 2007](#)), and, in particular, the anisotropic cardiac microstructure. One approach describes the heart as a single muscle coiled in a helical pattern, whereas the other approach considers the heart to be a continuum composed of laminar sheets, an approach we are adopting in the present work.

The left ventricle has the largest volume of the four chambers and serves the particular purpose of distributing blood with a higher pressure than the right ventricle. As a consequence of the need to support higher pressure, the wall thickness of the left ventricle is larger than that of the right ventricle. The wall thickness and curvature of the left ventricle vary spatially; it is thickest at the base and at the equator, and thinnest at its apex. The wall thickness and curvature also vary temporally through the cardiac cycle. The left ventricular wall may be regarded as a continuum of myocardial fibres, with a smooth transmural variation of the fibre orientations. It is modelled reasonably well as a thick-walled ellipsoid of revolution that is truncated at the base, as depicted in [figure 1a](#).

The heart wall consists of three distinct layers: an inner layer (the *endocardium*), a middle layer (the *myocardium*) and an outer layer (the *epicardium*). The endocardium lines the inside of the four chambers and it is a serous membrane, with approximate thickness 100 μm , consisting mainly of epimysial collagen, elastin and a layer of endothelial cells, the latter serving as an interfacial layer between the wall and the blood. The protective epicardium is also a membrane with thickness of the order of 100 μm and consists largely of epimysial collagen and some elastin.

In this paper, we focus our attention on the myocardium of the left ventricle. The ventricular myocardium is the functional tissue of the heart wall with a complex structure that is well represented in the quantitative studies of [LeGrice *et al.* \(1995, 1997\)](#), [Young *et al.* \(1998\)](#) and [Sands *et al.* \(2005\)](#). The left ventricular wall is a composite of layers (or sheets) of parallel myocytes, which are the predominant fibre types, occupying about 70 per cent of the volume. The remaining 30 per cent consists of various interstitial components ([Frank & Langer 1974](#)), whereas only 2–5 per cent of the interstitial volume is occupied by collagen arranged in a spatial network that forms lateral connections

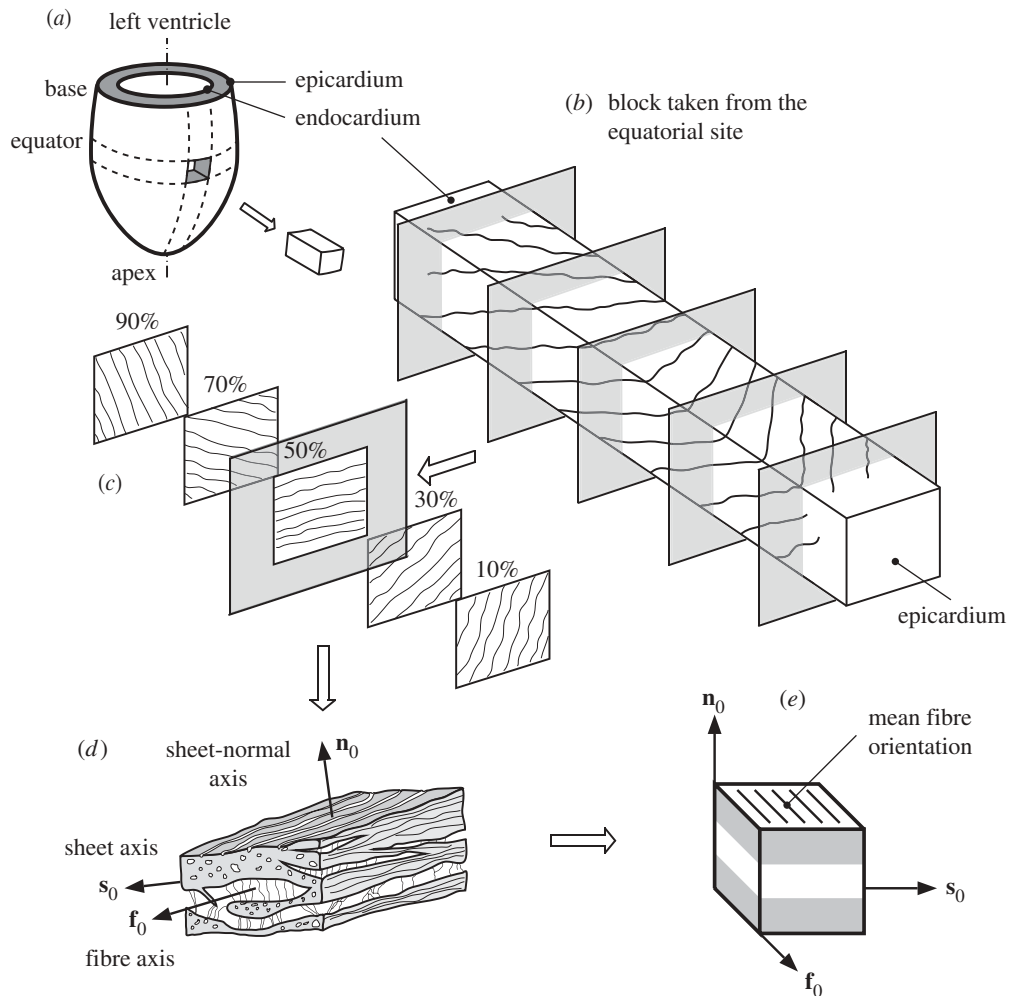


Figure 1. Schematic diagram of: (a) the left ventricle and a cutout from the equator; (b) the structure through the thickness from the epicardium to the endocardium; (c) five longitudinal–circumferential sections at regular intervals from 10 to 90 per cent of the wall thickness from the epicardium showing the transverse variation of layer orientation; (d) the layered organization of myocytes and the collagen fibres between the sheets referred to a right-handed orthonormal coordinate system with fibre axis \mathbf{f}_0 , sheet axis \mathbf{s}_0 and sheet-normal axis \mathbf{n}_0 ; and (e) a cube of layered tissue with local material coordinates (X_1, X_2, X_3) serving as the basis for the geometrical and constitutive model.

between adjacent muscle fibres, with attachments near the z-line of the sarcomere. Figure 1*b* illustrates the change of the three-dimensional layered organization of myocytes through the wall thickness from the epicardium to the endocardium. In addition, figure 1*c* displays views of five longitudinal–circumferential sections at regular intervals through the left ventricular wall (at 10–90% of the wall thickness from the epicardium). The sections are parallel to the epicardial surface and are displayed separately in figure 1*c*. As can be seen, the muscle fibre orientations change with position through the wall; in the equatorial region, the predominant

muscle fibre direction rotates from $+50^\circ$ to $+70^\circ$ (sub-epicardial region) to nearly 0° in the mid-wall region to -50° to -70° (sub-endocardial region) with respect to the circumferential direction of the left ventricle. It should be emphasized that the layers are not, in general, parallel to the vessel walls, as can be appreciated from [figure 1b](#) even though it is often assumed in the literature that they are so parallel.

[Figure 1d](#) is a schematic of the layered organization of myocytes with a fine weave of endomysial collagen surrounding the myocytes and lateral connections, which are 120–150 nm long, between adjacent myocytes. In addition, networks of long perimysial fibres span cleavage planes and connect adjacent muscle layers, which are three or four cells thick. The perimysial fibres are most likely to be the major structural elements of the extracellular matrix. They are coiled and have a ratio of contour length to end-to-end distance of approximately 1.3 in the unloaded state of the ventricle ([MacKenna et al. 1996](#)). Some branching between adjacent layers is evident, although, in many instances, branching is relatively sparse, so that the inter-layer separation can be significant. Capillaries with a fairly dense and uniform distribution within the myocardial layers and on their surfaces are also present, as indicated in [figure 1d](#). Understanding of the transmural variation of the myocardial tissue structure is important because this specific architecture is responsible for the resistance of the heart to bending and twisting during the cardiac cycle.

The layered organization is characterized by a right-handed orthonormal set of basis vectors and an associated orthogonal curvilinear system of coordinates. The local fixed set of (unit) basis vectors consists of the *fibre axis* \mathbf{f}_0 , which coincides with the muscle fibre orientation, the *sheet axis* \mathbf{s}_0 , defined to be in the plane of the layer perpendicular to the fibre direction (sometimes referred to as the cross-fibre direction), and the *sheet-normal axis* \mathbf{n}_0 , defined to be orthogonal to the other two. [Figure 1e](#), which shows a cube of layered tissue with the local material coordinates (X_1, X_2, X_3) , serves as a basis for the proposed geometrical and constitutive model. In what follows we shall use the labels f, s and n to refer to fibre, sheet and normal, respectively. We shall also use the pairs fs, fn and sn to refer to the fibre-sheet, fibre-normal and sheet-normal planes, respectively.

(b) Mechanical behaviour of the passive myocardium

The passive myocardium tissue is an orthotropic material having three mutually orthogonal planes with distinct material responses, as the results of [Dokos et al. \(2002\)](#) from *simple shear* tests on passive ventricular myocardium from pig hearts clearly show. This is illustrated in [figure 2](#), which is based on fig. 6 from the latter paper. It should be noted, however, that the ordering of the labels fn and fs in fig. 6 of [Dokos et al. \(2002\)](#) is inconsistent with the data shown in the other figures in that paper. To correct this, we have switched the roles of fs and fn in [figure 2](#) compared with fig. 6 of [Dokos et al. \(2002\)](#). This point is discussed further in §5d. The tissue exhibits a regionally dependent and time-dependent, highly nonlinear behaviour with relatively low hysteresis and also directionally dependent softening as the strain increases.

From [figure 2](#), it can be seen that ventricular myocardium is least resistant to simple shear in the fn and sn planes for shear in the f and s directions, respectively (the lowest curve in [figure 2](#) above the positive shear axis). It is

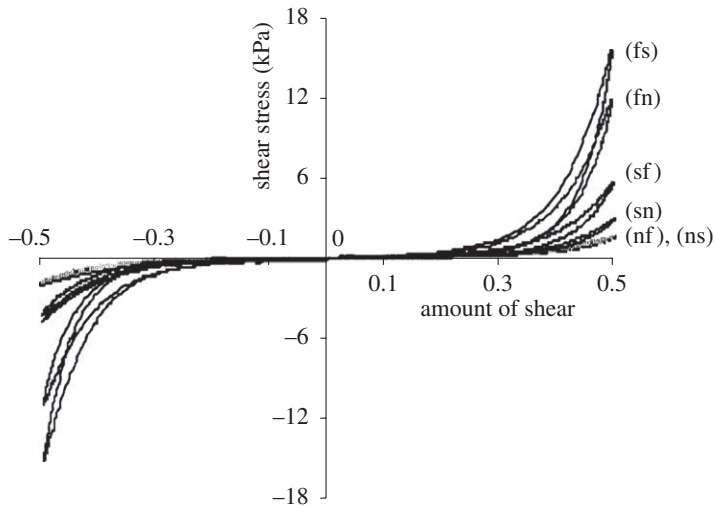


Figure 2. Shear stress versus amount of shear for simple shear tests on a cube of a typical myocardial specimen in the fs, fn and sn planes, where the (ij) shear refers to shear in the j direction in the ij plane, where $i \neq j \in \{f, s, n\}$. Note that the (ij) shear entails stretching of material line elements that are initially in the i direction. The data show clearly the distinct responses for the three planes and hence the orthotropy of the material. In addition, it illustrates the highly nonlinear response and the viscoelastic effect evidenced by the relatively small hysteresis between loading and unloading. For the planes containing the f direction, the shear responses (fs) and (fn) in the s and n directions are different; for the planes containing the s direction, the responses (sf) and (sn) in the f and n directions are also different; the shear responses (nf) and (ns) in the planes containing the n direction are the same for the considered specimen. Adapted from Dokos *et al.* (2002).

most resistant to shear deformations that produce extension of the myocyte (f) axis in the fs and fn planes (the upper two curves for positive shear). Note, however, that for the planes containing the fibre direction, the shear responses (fs) and (fn) in the sheet and normal directions are different. Similarly, for the planes containing the sheet direction, the responses (sf) and (sn) in the fibre and normal directions are different. On the other hand, the shear responses in the planes containing the normal direction are the same for the considered specimen.

The passive *biaxial* mechanical properties of non-contracting myocardium are described by Demer & Yin (1983), Yin *et al.* (1987), Smaill & Hunter (1991) and Novak *et al.* (1994), for example. To illustrate the results, we show in figure 3 representative stress–strain data that we extracted from fig. 4 in Yin *et al.* (1987). For three different loading protocols for biaxial loading in the fs plane of a canine left ventricle myocardium, figure 3*a* shows the second Piola–Kirchhoff stress S_{ff} in the fibre direction as a function of the Green–Lagrange strain E_{ff} in the same direction, whereas figure 3*b* shows the corresponding plots for the sheet direction (S_{ss} against E_{ss}). The three sets of data in figure 3*a,b* correspond to constant strain ratios E_{ff}/E_{ss} . Just as for the shear response, the biaxial data indicate high nonlinearity and anisotropy. Data for unloading were not given in Yin *et al.* (1987).

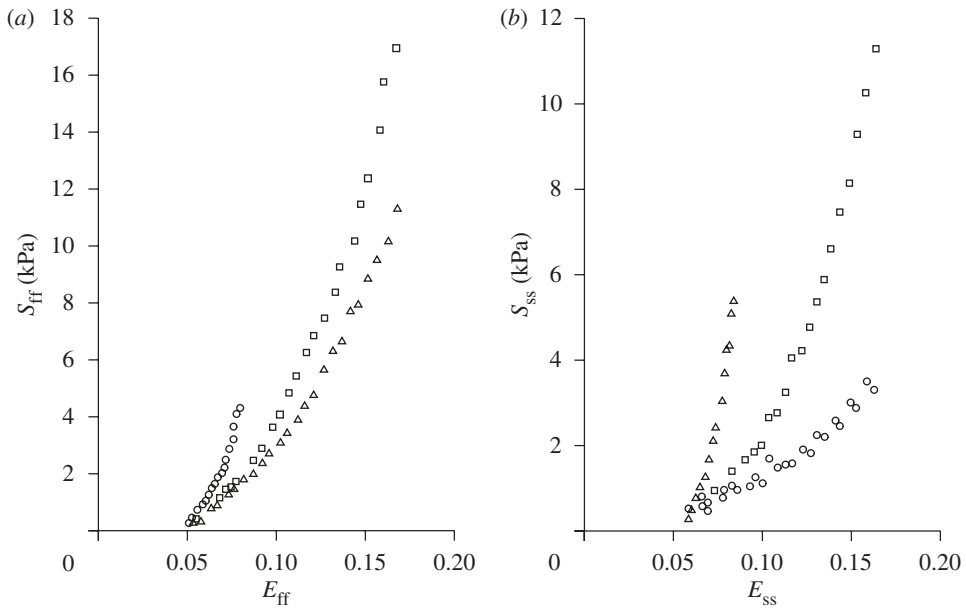


Figure 3. Representative stress–strain data for three different loading protocols for biaxial loading in the fs plane of canine left ventricle myocardium: (a) stress S_{ff} against strain E_{ff} in the fibre direction; (b) stress S_{ss} against strain E_{ss} in the sheet (cross-fibre) direction. Note that E_{ij} and S_{ij} are the components of the Green–Lagrange strain tensor and the second Piola–Kirchhoff stress tensor, respectively. The three sets of data correspond to constant strain ratios E_{ff}/E_{ss} equal to 2.05 (triangles), 1.02 (squares) and 0.48 (circles). The data are extracted from the two upper plots in fig. 4 of Yin *et al.* (1987).

As with many other soft biological tissues, the myocardium can be regarded as an incompressible material. This has been established in experiments by Vossoughi *et al.* (1980), who subjected tissue specimens to various levels of hydrostatic stress. They recorded the associated volumetric strains and concluded that the myocardial tissue is essentially incompressible.

According to experimental data obtained from equatorial slices of the left ventricular wall of potassium-arrested rat hearts, it is clear that the unloaded myocardium is residually stressed (Omens & Fung 1990) and, in particular, that there is compressive circumferential residual stress in the endocardium of the left ventricle and tensile circumferential residual stress in the epicardium; see also Costa *et al.* (1997), who suggested that the residual stress in the left ventricle is associated with pre-stretching in the plane of the myocardial sheets. According to Costa *et al.* (1997), there is relatively little residual stress along the muscle fibre direction in the mid-wall and there are also residual stresses normal to the fibre direction; the perimysial fibre network may be a primary residual stress-bearing structure in passive myocardium. Residual stresses are thought to arise during growth and remodelling (e.g. Rodriguez *et al.* 1994; Rachev 1997). Residual stresses have an important influence on the stress pattern in the typical physiological state. For example, incorporation of a residual stress distribution may reduce tensile endocardial stress concentrations predicted by

ventricular wall models (Guccione *et al.* 1991). The importance of residual stresses has also been recognized in arterial wall mechanics (e.g. Holzapfel *et al.* 2000; Holzapfel & Ogden 2003). However, three-dimensional residual stresses are very difficult to quantify and hence their modelling must be treated with caution.

Although the myocardium tissue appears to be viscoelastic, this aspect of its behaviour is not important from the point of view of mechanical modelling on the time scale of the cardiac cycle, which is short compared with the relaxation time of the viscoelastic response. Indeed, modelling of the viscoelasticity has received little attention in the literature, not least because there are very few data available on the viscoelastic properties of the tissue. An exception to this is the model of Huyghe *et al.* (1991). Here, we treat the tissue behaviour as elastic, with the characteristic features shown in figures 2 and 3.

It is therefore important to model the passive response of the left ventricular myocardium as a non-homogeneous, thick-walled, incompressible, orthotropic nonlinearly elastic material, and this is the approach we adopt in the present paper. Although residual stresses are also important for the stress analysis of the composite myocardium, it is first necessary to develop a constitutive model that takes full account of the basic structure of the material with respect to a stress-free reference configuration. Thus, we do not include residual stresses in the constitutive model developed here, as was the case for the arterial model constructed in Holzapfel *et al.* (2000).

3. Essential elements of continuum mechanics

(a) Kinematical quantities and invariants

The basic deformation variable for the description of the local kinematics is the deformation gradient \mathbf{F} , and we use the standard notation and convention

$$J = \det \mathbf{F} > 0. \quad (3.1)$$

For an incompressible material, we have the constraint

$$J = \det \mathbf{F} \equiv 1. \quad (3.2)$$

Associated with \mathbf{F} are the right and left Cauchy–Green tensors, defined by

$$\mathbf{C} = \mathbf{F}^T \mathbf{F} \quad \text{and} \quad \mathbf{B} = \mathbf{F} \mathbf{F}^T, \quad (3.3)$$

respectively. Also important for what follows is the Green–Lagrange (or Green) strain tensor, defined by

$$\mathbf{E} = \frac{1}{2}(\mathbf{C} - \mathbf{I}), \quad (3.4)$$

where \mathbf{I} is the identity tensor. The principal invariants of \mathbf{C} (and also of \mathbf{B}) are defined by

$$I_1 = \text{tr } \mathbf{C}, \quad I_2 = \frac{1}{2}[I_1^2 - \text{tr } (\mathbf{C}^2)] \quad \text{and} \quad I_3 = \det \mathbf{C}, \quad (3.5)$$

with $I_3 = J^2 = 1$ for an incompressible material. These are *isotropic* invariants. For more details of the relevant material from continuum mechanics, we refer to Holzapfel (2000) and Ogden (1997).

If the material has a preferred direction in the reference configuration, denoted by the unit vector \mathbf{a}_0 , this introduces anisotropy, specifically transverse isotropy, and with it come two additional (transversely isotropic) invariants (or quasi-invariants) defined by

$$I_4 = \mathbf{a}_0 \cdot (\mathbf{C}\mathbf{a}_0) \quad \text{and} \quad I_5 = \mathbf{a}_0 \cdot (\mathbf{C}^2\mathbf{a}_0). \quad (3.6)$$

Note that these are unaffected by reversal of the direction of \mathbf{a}_0 . If one wishes to distinguish between the directions \mathbf{a}_0 and $-\mathbf{a}_0$ as far as the material response is concerned, then yet another invariant would be needed. Here, however, we do not consider this possibility. We refer to [Spencer \(1984\)](#) for background information on the invariant theory of fibre-reinforced materials.

If there are two preferred directions, the second denoted by \mathbf{b}_0 , then this introduces the invariants

$$I_6 = \mathbf{b}_0 \cdot (\mathbf{C}\mathbf{b}_0) \quad \text{and} \quad I_7 = \mathbf{b}_0 \cdot (\mathbf{C}^2\mathbf{b}_0) \quad (3.7)$$

associated with it and, additionally, a coupling invariant, denoted by I_8 , which we define here by

$$I_8 = \mathbf{a}_0 \cdot (\mathbf{C}\mathbf{b}_0) = \mathbf{b}_0 \cdot (\mathbf{C}\mathbf{a}_0). \quad (3.8)$$

Note that this changes sign if either \mathbf{a}_0 or \mathbf{b}_0 (but not both) is reversed and is not therefore strictly invariant in this sense. However, it is more convenient in what follows to use this rather than the strictly invariant form I_8^2 or $I_8\mathbf{a}_0 \cdot \mathbf{b}_0$, and to allow for this distinction in the form of the constitutive law. Note that if $\mathbf{a}_0 \cdot \mathbf{b}_0 = 0$, then only the first of these two options is appropriate, but in this case I_8 depends on I_1, \dots, I_7 , specifically

$$I_8^2 = I_2 + I_4I_6 + I_5 + I_7 - I_1(I_4 + I_6), \quad (3.9)$$

a formula given in [Merodio & Ogden \(2006\)](#). Equation (3.9) determines only the magnitude of I_8 in terms of the other invariants, not its sign.

(b) Strain-energy function and stress tensors

Here we consider the material properties to be described by a strain-energy function Ψ , which is measured per unit reference volume. This depends on the deformation gradient \mathbf{F} through \mathbf{C} (equivalently through \mathbf{E}), which ensures objectivity. For such an elastic material, the Cauchy stress tensor $\boldsymbol{\sigma}$ is given by the formulae

$$J\boldsymbol{\sigma} = \mathbf{F} \frac{\partial \Psi}{\partial \mathbf{F}} = \mathbf{F} \frac{\partial \Psi}{\partial \mathbf{E}} \mathbf{F}^T \quad (3.10)$$

for a compressible material (for Ψ treated as a function of \mathbf{F} and \mathbf{E} , respectively), which are modified to

$$\boldsymbol{\sigma} = \mathbf{F} \frac{\partial \Psi}{\partial \mathbf{F}} - p\mathbf{I} = \mathbf{F} \frac{\partial \Psi}{\partial \mathbf{E}} \mathbf{F}^T - p\mathbf{I} \quad (3.11)$$

for an incompressible material, in which case we have the constraint $J = 1$ (equivalently $I_3 = J^2 = 1$) and this is accommodated in the expression for the stress by the Lagrange multiplier p .

For an elastic material possessing a strain-energy function Ψ that depends on a list of invariants, say I_1, I_2, \dots, I_N for some N , equations (3.10) and (3.11) may be expanded in the forms

$$\mathbf{J}\boldsymbol{\sigma} = \mathbf{F} \sum_{i=1}^N \psi_i \frac{\partial I_i}{\partial \mathbf{F}} \quad \text{and} \quad \boldsymbol{\sigma} = \mathbf{F} \sum_{i=1, i \neq 3}^N \psi_i \frac{\partial I_i}{\partial \mathbf{F}} - p\mathbf{I}, \quad (3.12)$$

respectively, where we have introduced the notation

$$\psi_i = \frac{\partial \Psi}{\partial I_i}, \quad i = 1, 2, \dots, N, \quad (3.13)$$

with $i=3$ omitted from the summation for the incompressible material and I_3 omitted from the list of invariants in Ψ in this case. Note that $\partial I_i / \partial \mathbf{F} = (\partial I_i / \partial \mathbf{E}) \mathbf{F}^T$ in terms of the Green–Lagrange strain tensor. Note that the second Piola–Kirchhoff stress tensor \mathbf{S} , whose components were referred to in connection with figure 3, is given in terms of the Cauchy stress tensor via the simple formula $\mathbf{S} = \mathbf{J} \mathbf{F}^{-1} \boldsymbol{\sigma} \mathbf{F}^{-T}$, using equation (3.10) for a compressible material and using equation (3.11) for an incompressible material with $J = 1$. Explicitly, with \mathbf{E} as the independent variable, we have simply

$$\mathbf{S} = \frac{\partial \Psi}{\partial \mathbf{E}} \quad \text{and} \quad \mathbf{S} = \frac{\partial \Psi}{\partial \mathbf{E}} - p(\mathbf{I} + 2\mathbf{E})^{-1} \quad (3.14)$$

for compressible and incompressible materials, respectively.

4. Review of existing constitutive models

For references to early work concerned with constitutive modelling of the myocardium, we refer to papers by Yin (1981) and Humphrey & Yin (1987). Several of the earlier models were based on linear isotropic elasticity, which is entirely inappropriate in view of the discussion in §2*b*. Equally, the early nonlinear models do not capture all the features alluded to. This is the case for certain invariant-based models, including the isotropic exponential form based on the invariant I_2 (Demiray 1976).

(a) Transversely isotropic models

A number of *transversely isotropic* models have been proposed. These include the model of Humphrey & Yin (1987), which is the sum of two exponentials, one in I_1 and one in I_4 , specifically

$$\Psi = c\{\exp[b(I_1 - 3)] - 1\} + A\{\exp[a(\sqrt{I_4} - 1)^2] - 1\}, \quad (4.1)$$

and contains four material parameters c , b , A and a . This was the first anisotropic invariant-based model that took account of the fibre structure. Another transversely isotropic model, also based on the invariants I_1 and I_4 , was constructed by Humphrey *et al.* (1990). This has the form

$$\Psi = c_1(\sqrt{I_4} - 1)^2 + c_2(\sqrt{I_4} - 1)^3 + c_3(I_1 - 3) + c_4(I_1 - 3)(\sqrt{I_4} - 1) + c_5(I_1 - 3)^2 \quad (4.2)$$

and involves five material constants c_1, c_2, \dots, c_5 , values of which were obtained by Novak *et al.* (1994) from biaxial test data from the middle portion of the inter-ventricular septum and the inner, middle and outer layers of the lateral passive canine left ventricle wall. As discussed in §2, it only subsequently became clear that the myocardium is not a transversely isotropic material (e.g. LeGrice *et al.* 1995).

The models referred to above are based on the assumption of incompressibility, but the shortcoming referred to above also applies to the compressible, transversely isotropic model due to Kerckhoffs *et al.* (2003), which has the form

$$\Psi = a_0[\exp(a_1\hat{I}_1^2 + a_2\hat{I}_2) - 1] + a_3[\exp(a_4E_{\text{ff}}^2) - 1] + a_5(I_3 - 1)^2, \quad (4.3)$$

and contains six material parameters a_0, a_1, \dots, a_5 , where \hat{I}_1 and \hat{I}_2 are the principal invariants of \mathbf{E} and E_{ff} is the Green–Lagrange strain in the fibre direction. The invariants \hat{I}_1 and \hat{I}_2 are related to the principal invariants I_1 and I_2 of \mathbf{C} defined in equation (3.5) by

$$\hat{I}_1 = \frac{1}{2}(I_1 - 3) \quad \text{and} \quad \hat{I}_2 = \frac{1}{4}(I_2 - 2I_1 + 3). \quad (4.4)$$

The first term in equation (4.3) represents the isotropic component related to tissue shape change, the second term relates to the extra stiffness of the material in the myofibre direction and finally the third term is related to volume changes.

Other transversely isotropic models, based on the use of the components of the Green–Lagrange strain tensor, were developed by Guccione *et al.* (1991) and Costa *et al.* (1996), but again do not reflect the morphology discussed above. They are both special cases of the orthotropic model of Costa *et al.* (2001) to be discussed below.

Some other models are structurally based. These include the model of Horowitz *et al.* (1988), which has the merit of being micro-mechanically motivated and inherently considers possible changes in the waviness of the fibres induced by the tissue strain. On the other hand, because of the integrations involved in the constitutive model, it is not well suited for numerical implementation. It is also effectively transversely isotropic.

The paper by Huyghe *et al.* (1991) contains one of the few models that characterize the passive *viscoelastic* response of the myocardium. It regards the material as sponge-like and treats it as a biphasic (fluid–solid) model based on the quasi-linear viscoelastic constitutive model due to Fung (1993, §7.6) and, to our knowledge, is the only biphasic model of the myocardium documented in the literature. The model has been implemented within a finite element framework and applied to the left ventricle of a canine diastolic heart in Huyghe *et al.* (1992). Of interest here is the solid elastic phase, which is a *transversely isotropic* model involving seven material parameters. However, the authors refer to it as *orthotropic*. That it is transversely isotropic can be seen from eq. (B 8) in appendix B of Huyghe *et al.* (1992) by noting that their strain-energy function is invariant under interchange of the indices 1 and 2, and hence with respect to rotations about the 3 direction.

(b) *Orthotropic models*

Several *orthotropic* models have been proposed in the literature. Some of these are inappropriate for modelling myocardial tissue, including the Langevin eight-chain based model of Bischoff *et al.* (2002), which, as pointed out by Schmid *et al.* (2008), does not reflect the morphology of the myocardium.

In the remainder of this section, we describe briefly three orthotropic models that have similar features in that they are partly structurally based, relating to the fibre, sheet and normal directions, and partly phenomenological. This is a prelude to the development, in §5, of a general orthotropic invariant-based model, which includes these three models as special cases.

Note that, in the models listed in §4*b*(i)–(iii) below, the authors have used the notation E_{ij} with $i, j \in \{f, s, n\}$, and, in particular, although $E_{ij} = E_{ji}$, they have expressed the off-diagonal terms in the form $(E_{ij} + E_{ji})/2$, where $i \neq j$. Here, for compactness, we simply express this as E_{ij} in each case.

(i) *Strain-energy function proposed by Costa et al. (2001)*

The Fung-type exponential strain-energy function due to Costa *et al.* (2001) is given by

$$\Psi = \frac{1}{2}a(\exp Q - 1), \quad (4.5)$$

where

$$Q = b_{ff}E_{ff}^2 + b_{ss}E_{ss}^2 + b_{nn}E_{nn}^2 + 2b_{fs}E_{fs}^2 + 2b_{fn}E_{fn}^2 + 2b_{sn}E_{sn}^2, \quad (4.6)$$

which has seven material parameters, a and b_{ij} , where $i, j \in \{f, s, n\}$. Interpretations were given for the parameters, but specific values were not provided. As already mentioned, transversely isotropic specializations of this model (with five material parameters) were used in earlier papers by Guccione *et al.* (1991) and Costa *et al.* (1996).

(ii) *Fung-type model proposed by Schmid et al. (2006)*

Another Fung-type model consisting of separate exponential terms for each component E_{ij} was introduced by Schmid *et al.* (2006) to decouple the effects of the material parameters in the single-exponential model (4.5) and (4.6). With 12 material parameters, it is given by

$$\begin{aligned} \Psi = & \frac{1}{2}a_{ff}[\exp(b_{ff}E_{ff}^2) - 1] + \frac{1}{2}a_{fn}[\exp(b_{fn}E_{fn}^2) - 1] + \frac{1}{2}a_{fs}[\exp(b_{fs}E_{fs}^2) - 1] \\ & + \frac{1}{2}a_{nn}[\exp(b_{nn}E_{nn}^2) - 1] + \frac{1}{2}a_{ns}[\exp(b_{ns}E_{ns}^2) - 1] + \frac{1}{2}a_{ss}[\exp(b_{ss}E_{ss}^2) - 1]. \end{aligned} \quad (4.7)$$

We mention in passing another model with 12 parameters, which also uses the components E_{ij} , where $i, j \in \{f, s, n\}$. This is the tangent model introduced in Schmid *et al.* (2006); see also Schmid *et al.* (2008). We do not consider this model here.

(iii) *Pole-zero model proposed by Hunter et al. (1997)*

Motivated by the (equi-)biaxial tension tests of Smaill & Hunter (1991), Hunter *et al.* (1997) proposed the so-called *pole-zero* strain-energy function, which has the form

$$\begin{aligned} \Psi = & \frac{k_{\text{ff}} E_{\text{ff}}^2}{|a_{\text{ff}} - |E_{\text{ff}}||^{b_{\text{ff}}}} + \frac{k_{\text{fn}} E_{\text{fn}}^2}{|a_{\text{fn}} - |E_{\text{fn}}||^{b_{\text{fn}}}} + \frac{k_{\text{nn}} E_{\text{nn}}^2}{|a_{\text{nn}} - |E_{\text{nn}}||^{b_{\text{nn}}}} \\ & + \frac{k_{\text{fs}} E_{\text{fs}}^2}{|a_{\text{fs}} - |E_{\text{fs}}||^{b_{\text{fs}}}} + \frac{k_{\text{ss}} E_{\text{ss}}^2}{|a_{\text{ss}} - |E_{\text{ss}}||^{b_{\text{ss}}}} + \frac{k_{\text{ns}} E_{\text{ns}}^2}{|a_{\text{ns}} - |E_{\text{ns}}||^{b_{\text{ns}}}} \end{aligned} \quad (4.8)$$

with 18 material parameters k_{ij} , a_{ij} and b_{ij} , where $i, j \in \{\text{f}, \text{s}, \text{n}\}$, and with different components E_{ij} separated similarly to equation (4.7). As mentioned in Nash (1998), it was considered unlikely to be suitable for other modes of deformation. Note that several different forms of this model appear in various papers with or without appropriate modulus signs, and in some cases with b_{ij} set equal to 2 for each i, j pair, as in Schmid *et al.* (2006, 2008).

The relative performance of the above orthotropic models in fitting data of Dokos *et al.* (2002) was evaluated in Schmid *et al.* (2008), and we discuss this briefly in §7.

5. A structurally based model for the passive myocardium

Bearing in mind the fibre, sheet (cross-fibre) and sheet-normal (normal) directions specified in figure 1*e* and the definition of the invariant I_4 in the first part of equation (3.6), we now consider the invariant I_4 associated with each of these directions. We use the notation

$$I_{4\text{f}} = \mathbf{f}_0 \cdot (\mathbf{C}\mathbf{f}_0), \quad I_{4\text{s}} = \mathbf{s}_0 \cdot (\mathbf{C}\mathbf{s}_0) \quad \text{and} \quad I_{4\text{n}} = \mathbf{n}_0 \cdot (\mathbf{C}\mathbf{n}_0) \quad (5.1)$$

and note that

$$\sum_{i=\text{f}, \text{s}, \text{n}} I_{4i} = \mathbf{C} : (\mathbf{f}_0 \otimes \mathbf{f}_0 + \mathbf{s}_0 \otimes \mathbf{s}_0 + \mathbf{n}_0 \otimes \mathbf{n}_0) = \mathbf{C} : \mathbf{I} = I_1. \quad (5.2)$$

Thus, only three of the invariants $I_{4\text{f}}$, $I_{4\text{s}}$, $I_{4\text{n}}$ and I_1 are independent, and in the functional dependence of the strain energy we may omit one of these.

On the basis of the definition for the second part of equation (3.6), we may also define invariants $I_{5\text{f}}$, $I_{5\text{s}}$ and $I_{5\text{n}}$ for each direction. We shall not need these here, but we note that they are related by $I_{5\text{f}} + I_{5\text{s}} + I_{5\text{n}} = I_1^2 - 2I_2$. Additionally, there are the coupling invariants associated with the pairs of directions. In accordance with the definition (3.8), we may write

$$I_{8\text{fs}} = I_{8\text{sf}} = \mathbf{f}_0 \cdot (\mathbf{C}\mathbf{s}_0), \quad I_{8\text{fn}} = I_{8\text{nf}} = \mathbf{f}_0 \cdot (\mathbf{C}\mathbf{n}_0) \quad \text{and} \quad I_{8\text{sn}} = I_{8\text{ns}} = \mathbf{s}_0 \cdot (\mathbf{C}\mathbf{n}_0). \quad (5.3)$$

In what follows, we shall make use of these. In fact, it is not difficult to show that $I_{5\text{f}}$, $I_{5\text{s}}$ and $I_{5\text{n}}$ are expressible in terms of the other invariants via

$$I_{5\text{f}} = I_{4\text{f}}^2 + I_{8\text{fs}}^2 + I_{8\text{fn}}^2, \quad I_{5\text{s}} = I_{4\text{s}}^2 + I_{8\text{fs}}^2 + I_{8\text{sn}}^2 \quad \text{and} \quad I_{5\text{n}} = I_{4\text{n}}^2 + I_{8\text{fn}}^2 + I_{8\text{sn}}^2 \quad (5.4)$$

and that

$$I_{4\text{f}} I_{4\text{s}} I_{4\text{n}} - I_{4\text{f}} I_{8\text{sn}}^2 - I_{4\text{s}} I_{8\text{fn}}^2 - I_{4\text{n}} I_{8\text{fs}}^2 + 2I_{8\text{fs}} I_{8\text{fn}} I_{8\text{sn}} = I_3. \quad (5.5)$$

Thus, if the material is compressible, there are seven independent invariants, whereas for an incompressible material there are only six. These numbers compare with the eight (compressible) and seven (incompressible) for the case of a material with two *non-orthogonal* preferred directions. The orthogonality here reduces the number of invariants by one.

Note that, in terms of the components E_{ij} , where $i, j \in \{f, s, n\}$, of the Green–Lagrange strain tensor used in several of the models discussed in §4, we have the connections $2E_{ii} = I_{4i} - 1$, where $i \in \{f, s, n\}$ (no summation over i), and $2E_{ij} = I_{8ij}$, where $i \neq j$. Thus, the general framework herein embraces the orthotropic models discussed in §4 as special cases.

Before we consider the most general case, we note that, for a compressible material that depends only on the invariants I_1 , I_{4f} , I_{4s} and I_3 , for example, the first formula in (3.12) yields

$$J\boldsymbol{\sigma} = 2\psi_1\mathbf{B} + 2\psi_{4f}\mathbf{f} \otimes \mathbf{f} + 2\psi_{4s}\mathbf{s} \otimes \mathbf{s} + 2I_3\psi_3\mathbf{I}, \quad (5.6)$$

where $\mathbf{B} = \mathbf{F}\mathbf{F}^T$, $\mathbf{f} = \mathbf{F}\mathbf{f}_0$, $\mathbf{s} = \mathbf{F}\mathbf{s}_0$ and $\psi_{4i} = \partial\Psi/\partial I_{4i}$, where $i = f, s$. We shall also use the notation $\mathbf{n} = \mathbf{F}\mathbf{n}_0$. The counterpart of the formula (5.6) for an incompressible material is

$$\boldsymbol{\sigma} = 2\psi_1\mathbf{B} + 2\psi_{4f}\mathbf{f} \otimes \mathbf{f} + 2\psi_{4s}\mathbf{s} \otimes \mathbf{s} - p\mathbf{I}. \quad (5.7)$$

Note that here we have omitted the invariant I_{4n} rather than I_1 , I_{4f} or I_{4s} . There is a good physical reason for this choice, as we will explain in §6.

(a) Application to simple shear

Consider now simple shear in different planes and choose the axes so that the component vectors are given by

$$[\mathbf{f}_0] = [1 \ 0 \ 0]^T, \quad [\mathbf{s}_0] = [0 \ 1 \ 0]^T \quad \text{and} \quad [\mathbf{n}_0] = [0 \ 0 \ 1]^T. \quad (5.8)$$

We now consider simple shear separately in each of the three planes fs , sn and fn , and we identify the indices 1, 2 and 3 with f , s and n , respectively (figure 4).

(i) Shear in the fs plane

We begin with simple shear in the fs plane and consider separately shear in the \mathbf{f}_0 and \mathbf{s}_0 directions. For shears in the \mathbf{f}_0 and \mathbf{s}_0 directions, the deformation gradients have components

$$[\mathbf{F}] = \begin{bmatrix} 1 & \gamma & 0 \\ 0 & 1 & 0 \\ 0 & 0 & 1 \end{bmatrix} \quad \text{and} \quad [\mathbf{F}] = \begin{bmatrix} 1 & 0 & 0 \\ \gamma & 1 & 0 \\ 0 & 0 & 1 \end{bmatrix}, \quad (5.9)$$

respectively. For the shear in the \mathbf{f}_0 direction, we obtain

$$[\mathbf{B}] = \begin{bmatrix} 1 + \gamma^2 & \gamma & 0 \\ \gamma & 1 & 0 \\ 0 & 0 & 1 \end{bmatrix}, \quad \mathbf{f} = \mathbf{f}_0, \quad \mathbf{s} = \gamma\mathbf{f}_0 + \mathbf{s}_0, \quad \mathbf{n} = \mathbf{n}_0, \quad (5.10)$$

$I_{4s} = 1 + \gamma^2$, $I_{4f} = I_{4n} = 1$, the active shear stress is $\sigma_{12} = 2\gamma(\psi_1 + \psi_{4s})$ and $\sigma_{13} = \sigma_{23} = 0$.

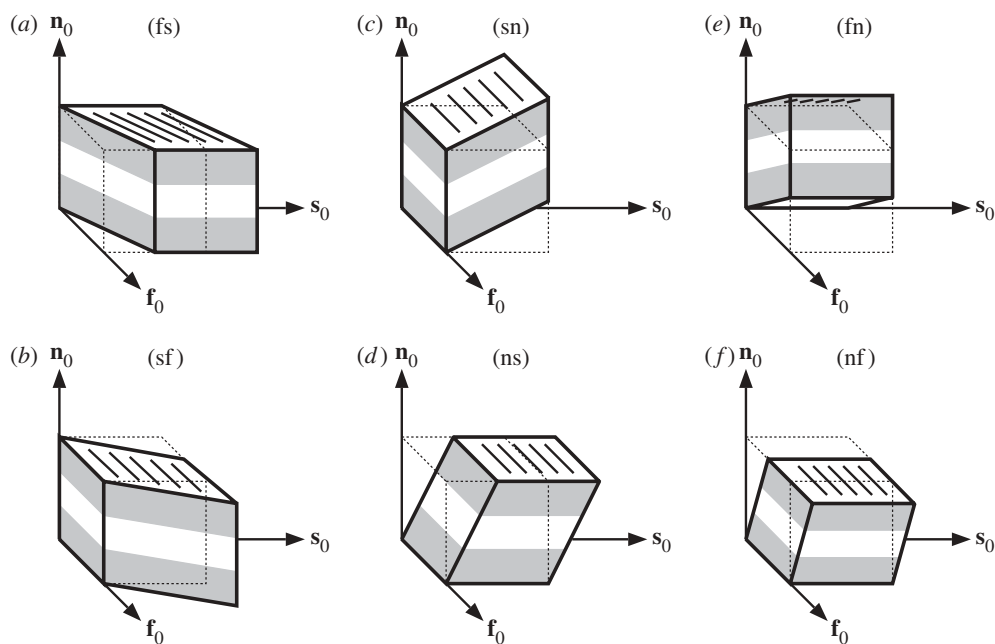


Figure 4. Sketches of six possible modes of simple shear for myocardium defined with respect to the fibre axis \mathbf{f}_0 , sheet axis \mathbf{s}_0 and sheet-normal axis \mathbf{n}_0 : each mode is a plane strain deformation. The modes are designated (ij) , where $i, j \in \{f, s, n\}$, corresponding to shear in the ij plane with shear in the j direction. Thus, the first letter in (ij) denotes the normal vector of the face that is shifted by the simple shear, whereas the second denotes the direction in which that face is shifted. The modes in which the fibres are stretched are (fn) and (fs) .

For the shear in the \mathbf{s}_0 direction, we have

$$[\mathbf{B}] = \begin{bmatrix} 1 & \gamma & 0 \\ \gamma & 1 + \gamma^2 & 0 \\ 0 & 0 & 1 \end{bmatrix}, \quad \mathbf{f} = \mathbf{f}_0 + \gamma \mathbf{s}_0, \quad \mathbf{s} = \mathbf{s}_0, \quad \mathbf{n} = \mathbf{n}_0, \quad (5.11)$$

$I_{4f} = 1 + \gamma^2$, $I_{4s} = I_{4n} = 1$, the active shear stress is $\sigma_{12} = 2\gamma(\psi_1 + \psi_{4f})$ and again $\sigma_{13} = \sigma_{23} = 0$. Hence, the two shear responses in the fs plane are different. Note that, for each of the above two cases, $I_{8fs} = \gamma$ and $I_{8fn} = I_{8sn} = 0$.

(ii) Shear in the sn plane

Next, we consider simple shear in the sn plane, considering separately shear in the \mathbf{s}_0 and \mathbf{n}_0 directions. Shears in the \mathbf{s}_0 and \mathbf{n}_0 directions have deformation gradients with components

$$[\mathbf{F}] = \begin{bmatrix} 1 & 0 & 0 \\ 0 & 1 & \gamma \\ 0 & 0 & 1 \end{bmatrix} \quad \text{and} \quad [\mathbf{F}] = \begin{bmatrix} 1 & 0 & 0 \\ 0 & 1 & 0 \\ 0 & \gamma & 1 \end{bmatrix}, \quad (5.12)$$

respectively. For the shear in the \mathbf{s}_0 direction, we have

$$[\mathbf{B}] = \begin{bmatrix} 1 & 0 & 0 \\ 0 & 1 + \gamma^2 & \gamma \\ 0 & \gamma & 1 \end{bmatrix}, \quad \mathbf{f} = \mathbf{f}_0, \quad \mathbf{s} = \mathbf{s}_0, \quad \mathbf{n} = \mathbf{n}_0 + \gamma \mathbf{s}_0, \quad (5.13)$$

$I_{4n} = 1 + \gamma^2$, $I_{4f} = I_{4s} = 1$, the active shear stress is $\sigma_{23} = 2\gamma\psi_1$ and $\sigma_{12} = \sigma_{13} = 0$.

For the shear in the \mathbf{n}_0 direction, we obtain

$$[\mathbf{B}] = \begin{bmatrix} 1 & 0 & 0 \\ 0 & 1 & \gamma \\ 0 & \gamma & 1 + \gamma^2 \end{bmatrix}, \quad \mathbf{f} = \mathbf{f}_0, \quad \mathbf{s} = \mathbf{s}_0 + \gamma \mathbf{n}_0, \quad \mathbf{n} = \mathbf{n}_0, \quad (5.14)$$

$I_{4s} = 1 + \gamma^2$, $I_{4f} = I_{4n} = 1$, the active shear stress is $\sigma_{23} = 2\gamma(\psi_1 + \psi_{4s})$ and $\sigma_{12} = \sigma_{13} = 0$. Hence, the two shear responses in the \mathbf{sn} plane are different. Note that, for each of the above two cases, $I_{8sn} = \gamma$ and $I_{8fs} = I_{8fn} = 0$.

(iii) Shear in the \mathbf{fn} plane

Finally, we have simple shear in the \mathbf{fn} plane. For shears in the \mathbf{f}_0 and \mathbf{n}_0 directions, the deformation gradients are

$$[\mathbf{F}] = \begin{bmatrix} 1 & 0 & \gamma \\ 0 & 1 & 0 \\ 0 & 0 & 1 \end{bmatrix} \quad \text{and} \quad [\mathbf{F}] = \begin{bmatrix} 1 & 0 & 0 \\ 0 & 1 & 0 \\ \gamma & 0 & 1 \end{bmatrix}, \quad (5.15)$$

respectively. For the shear in the \mathbf{f}_0 direction, we have

$$[\mathbf{B}] = \begin{bmatrix} 1 + \gamma^2 & 0 & \gamma \\ 0 & 1 & 0 \\ \gamma & 0 & 1 \end{bmatrix}, \quad \mathbf{f} = \mathbf{f}_0, \quad \mathbf{s} = \mathbf{s}_0, \quad \mathbf{n} = \mathbf{n}_0 + \gamma \mathbf{f}_0, \quad (5.16)$$

$I_{4n} = 1 + \gamma^2$, $I_{4f} = I_{4s} = 1$, the active shear stress is $\sigma_{13} = 2\gamma\psi_1$ and $\sigma_{12} = \sigma_{23} = 0$.

For the shear in the \mathbf{n}_0 direction, we have

$$[\mathbf{B}] = \begin{bmatrix} 1 & 0 & \gamma \\ 0 & 1 & 0 \\ \gamma & 0 & 1 + \gamma^2 \end{bmatrix}, \quad \mathbf{f} = \mathbf{f}_0 + \gamma \mathbf{n}_0, \quad \mathbf{s} = \mathbf{s}_0, \quad \mathbf{n} = \mathbf{n}_0, \quad (5.17)$$

$I_{4f} = 1 + \gamma^2$, $I_{4s} = I_{4n} = 1$, the active shear stress is $\sigma_{13} = 2\gamma(\psi_1 + \psi_{4f})$ and $\sigma_{12} = \sigma_{23} = 0$. Hence, the two shear responses in the \mathbf{fn} plane are different. Note that, for each of the above two cases, $I_{8fn} = \gamma$ and $I_{8fs} = I_{8sn} = 0$.

Clearly, the (nf) and (ns) shear responses are the same, where we now recall that we use the notation (ij) to specify that the shear is in the j direction in the ij plane, with $i, j \in \{f, s, n\}$. In these two cases, there is stretching along the \mathbf{n}_0 direction, but not along the \mathbf{f}_0 or \mathbf{s}_0 directions. The (sn) and (sf) shear responses are also the same, with no stretching along the \mathbf{f}_0 or \mathbf{n}_0 direction and, finally, the responses are also the same in the fs and fn planes, with stretching along the fibre direction \mathbf{f}_0 in these cases. It should also be emphasized that, in the above, the order of the indices i and j in (ij) (when referring to *shear* or *response*) is important, but without parentheses, in ij , the order is not relevant (when referring to *plane*).

The data of Dokos *et al.* (2002) indicate that the shear response is stiffest when the fibre direction is extended, least stiff when the normal direction is extended and has intermediate stiffness when the sheet direction is extended. This is reflected by the above formulae for the shear stresses if $\psi_{4f} > \psi_{4s} > 0$. However, the data also show that there are differences between the (fs) and (fn) and between the (sf) and (sn) responses, which are not captured by the above model; the data also show that the (nf) and (ns) responses are indistinguishable. A possible way to refine the model in order to reflect these differences is to include in the strain-energy function one or more of the coupling invariants defined in equation (5.3). Bearing in mind that the most general strain-energy function depends only on seven invariants for a compressible material, we may select, for example, $I_1, I_2, I_3, I_{4f}, I_{4s}, I_{8fs}$ and I_{8fn} , in which case the Cauchy stress (5.6) is given by

$$\begin{aligned} J\boldsymbol{\sigma} = & 2\psi_1\mathbf{B} + 2\psi_2(I_1\mathbf{B} - \mathbf{B}^2) + 2I_3\psi_3\mathbf{I} + 2\psi_{4f}\mathbf{f} \otimes \mathbf{f} + 2\psi_{4s}\mathbf{s} \otimes \mathbf{s} \\ & + \psi_{8fs}(\mathbf{f} \otimes \mathbf{s} + \mathbf{s} \otimes \mathbf{f}) + \psi_{8fn}(\mathbf{f} \otimes \mathbf{n} + \mathbf{n} \otimes \mathbf{f}). \end{aligned} \quad (5.18)$$

We emphasize that the invariants I_{8fs} and I_{8fn} appearing in equation (5.18), and also I_{8sn} , depend on the *sense* of $\mathbf{f}_0, \mathbf{s}_0$ and \mathbf{n}_0 , i.e. they change sign if the sense of one of the vectors is reversed. However, Ψ should be independent of this sense and this is accommodated by an appropriate functional dependence. For example, if we write $\hat{\Psi}(\dots, I_{8fs}^2, \dots) = \Psi(\dots, I_{8fs}, \dots)$, then $\psi_{8fs} = 2\partial\hat{\Psi}/\partial(I_{8fs}^2)I_{8fs}$ and for shear in the fs plane we have $I_{8fs} = \mathbf{f} \cdot \mathbf{s} = \gamma$ for either direction of shear, and this vanishes in the reference configuration, as does ψ_{8fs} provided Ψ is well behaved as a function of I_{8fs}^2 (which we assume to be the case). Similarly, $I_{8fn} = \mathbf{f} \cdot \mathbf{n} = \gamma$ for shear in the fn plane and $I_{8sn} = \mathbf{s} \cdot \mathbf{n} = \gamma$ for shear in the sn plane.

In view of the above, in the reference configuration, equation (5.18) reduces to

$$2(\psi_1 + 2\psi_2 + \psi_3)\mathbf{I} + 2\psi_{4f}\mathbf{f}_0 \otimes \mathbf{f}_0 + 2\psi_{4s}\mathbf{s}_0 \otimes \mathbf{s}_0 = \mathbf{0}, \quad (5.19)$$

assuming the reference configuration is stress-free, and this can hold only if

$$\psi_1 + 2\psi_2 + \psi_3 = 0, \quad \psi_{4f} = 0 \quad \text{and} \quad \psi_{4s} = 0. \quad (5.20)$$

Thus, these conditions must be satisfied along with

$$\psi_{8fs} = \psi_{8fn} = 0 \quad (5.21)$$

in the reference configuration.

For an incompressible material, equation (5.18) is replaced by

$$\begin{aligned} \boldsymbol{\sigma} = & 2\psi_1\mathbf{B} + 2\psi_2(I_1\mathbf{B} - \mathbf{B}^2) - p\mathbf{I} + 2\psi_{4f}\mathbf{f} \otimes \mathbf{f} + 2\psi_{4s}\mathbf{s} \otimes \mathbf{s} \\ & + \psi_{8fs}(\mathbf{f} \otimes \mathbf{s} + \mathbf{s} \otimes \mathbf{f}) + \psi_{8fn}(\mathbf{f} \otimes \mathbf{n} + \mathbf{n} \otimes \mathbf{f}) \end{aligned} \quad (5.22)$$

and only the six invariants $I_1, I_2, I_{4f}, I_{4s}, I_{8fs}$ and I_{8fn} remain. In this case, the conditions that must be satisfied in the reference configuration are as above except for the first equation in (5.20), which is replaced by $2\psi_1 + 4\psi_2 - p_0 = 0$, where p_0 is the value of p in the reference configuration.

For simple shear in the fs plane, the term in $\psi_{8\text{fs}}$ contributes $\psi_{8\text{fs}}$ to σ_{12} for shear in either the \mathbf{f}_0 or \mathbf{s}_0 direction, but does not contribute if the shear is in either the fn or sn plane. Similarly, the term in $\psi_{8\text{fn}}$ contributes $\psi_{8\text{fn}}$ to σ_{13} for shear in either the \mathbf{f}_0 or \mathbf{n}_0 direction in the fn plane. Also, as noted above, because the dependence of Ψ is on the square of each of these invariants, each of these two terms involves a factor of γ .

In summary, the equations for shear stress versus amount of shear for the six simple shears enumerated in §5*a*(i)–(iii) are given by

$$(\text{fs}): \quad \sigma_{\text{fs}} = 2(\psi_1 + \psi_2 + \psi_{4\text{f}})\gamma + \psi_{8\text{fs}}, \quad (5.23)$$

$$(\text{fn}): \quad \sigma_{\text{fn}} = 2(\psi_1 + \psi_2 + \psi_{4\text{f}})\gamma + \psi_{8\text{fn}}, \quad (5.24)$$

$$(\text{sf}): \quad \sigma_{\text{fs}} = 2(\psi_1 + \psi_2 + \psi_{4\text{s}})\gamma + \psi_{8\text{fs}}, \quad (5.25)$$

$$(\text{sn}): \quad \sigma_{\text{sn}} = 2(\psi_1 + \psi_2 + \psi_{4\text{s}})\gamma, \quad (5.26)$$

$$(\text{nf}): \quad \sigma_{\text{fn}} = 2(\psi_1 + \psi_2)\gamma + \psi_{8\text{fn}} \quad (5.27)$$

$$\text{and} \quad (\text{ns}): \quad \sigma_{\text{sn}} = 2(\psi_1 + \psi_2)\gamma. \quad (5.28)$$

It is worth remarking here that, as simple shear is a plane strain deformation, the invariants I_1 and I_2 are identical and the effects of ψ_1 and ψ_2 cannot be distinguished.

(b) Application to biaxial deformation

Several experiments have been conducted using biaxial tests on thin sheets of tissue taken from planes parallel to the endocardium. Such specimens are purportedly from within a sheet containing the fibre axis and the in-sheet axis. These are referred to as the fibre and cross-fibre directions. Note, however, that, according to the structure discussed in §2, such specimens are, in general, unlikely to contain a specific myocyte sheet, so care must be exercised in interpreting such biaxial data.

Consider the pure homogeneous deformation defined by

$$x_1 = \lambda_{\text{f}} X_1, \quad x_2 = \lambda_{\text{s}} X_2 \quad \text{and} \quad x_3 = \lambda_{\text{n}} X_3, \quad (5.29)$$

where λ_{f} , λ_{s} and λ_{n} are the principal stretches, identified with the fibre, sheet and normal directions, respectively. They satisfy the incompressibility condition

$$\lambda_{\text{f}} \lambda_{\text{s}} \lambda_{\text{n}} = 1. \quad (5.30)$$

When the deformation (5.29) is applied to a thin sheet of tissue parallel to a sheet with no lateral stress, there is no shear strain and hence $I_{8\,ij} = 0$, where $i \neq j \in \{\text{f}, \text{s}, \text{n}\}$, and $\psi_{8\,ij} = 0$ correspondingly. Equation (5.22) then has only three components, namely

$$\sigma_{\text{ff}} = 2\psi_1 \lambda_{\text{f}}^2 + 2\psi_2 (\lambda_{\text{s}}^2 + \lambda_{\text{n}}^2) \lambda_{\text{f}}^2 + 2\psi_{4\text{f}} \lambda_{\text{f}}^2 - p, \quad (5.31)$$

$$\sigma_{\text{ss}} = 2\psi_1 \lambda_{\text{s}}^2 + 2\psi_2 (\lambda_{\text{n}}^2 + \lambda_{\text{f}}^2) \lambda_{\text{s}}^2 + 2\psi_{4\text{s}} \lambda_{\text{s}}^2 - p \quad (5.32)$$

$$\text{and} \quad 0 = 2\psi_1 \lambda_{\text{n}}^2 + 2\psi_2 (\lambda_{\text{f}}^2 + \lambda_{\text{s}}^2) \lambda_{\text{n}}^2 - p. \quad (5.33)$$

Elimination of p by means of equation (5.33) allows equations (5.31) and (5.32) to be expressed as

$$\sigma_{\text{ff}} = 2\psi_1(\lambda_{\text{f}}^2 - \lambda_{\text{n}}^2) + 2\psi_2\lambda_{\text{s}}^2(\lambda_{\text{f}}^2 - \lambda_{\text{n}}^2) + 2\psi_{4\text{f}}\lambda_{\text{f}}^2 \quad (5.34)$$

and
$$\sigma_{\text{ss}} = 2\psi_1(\lambda_{\text{s}}^2 - \lambda_{\text{n}}^2) + 2\psi_2\lambda_{\text{f}}^2(\lambda_{\text{s}}^2 - \lambda_{\text{n}}^2) + 2\psi_{4\text{s}}\lambda_{\text{s}}^2. \quad (5.35)$$

If we omit the dependence on the invariant I_2 , then the last two equations simplify to

$$\sigma_{\text{ff}} = 2\psi_1(\lambda_{\text{f}}^2 - \lambda_{\text{n}}^2) + 2\psi_{4\text{f}}\lambda_{\text{f}}^2 \quad (5.36)$$

and
$$\sigma_{\text{ss}} = 2\psi_1(\lambda_{\text{s}}^2 - \lambda_{\text{n}}^2) + 2\psi_{4\text{s}}\lambda_{\text{s}}^2. \quad (5.37)$$

(c) A specific model

To decide which of the invariants to include in a particular model, we now examine interpretations of the invariants. First, we include an isotropic term based on the invariant I_1 because this can be regarded as associated with the underlying non-collagenous and non-muscular matrix (which includes fluids). This could be modelled as a neo-Hookean material, as in the case of arteries (Holzapfel *et al.* 2000), or as an exponential (Demiray 1972), for example.

A schematic of the embedded collagen–muscle fibre structure is shown in figure 5 for the unloaded configuration and, separately, for configurations subject to tension and compression in the direction of the muscle fibre (cardiac myocyte). The collagen fibres illustrated in figure 5 are thought to represent both the endomysial and the perimysial collagen fibres, as briefly described in §2a. Figure 5b, in particular, shows the configuration in which the tensile loading is in the muscle fibre direction. The muscle fibres are extended and the inter-fibre distances are decreased, while the collagenous network offers little resistance laterally but does contribute to the exponentially increasing stress in the muscle fibre direction. For tensile loading lateral to the muscle fibres, there is also exponential stress stiffening, which can be thought of as being generated by recruitment of the collagen network. Figure 5c depicts the tendency of the muscle fibres to buckle under compressive load in the muscle fibre direction and stretched collagen cross-fibres, i.e. the lateral inter-fibre connections as well as the woven perimysial network are stretched. It is suggested that the lateral stretching of the collagen fibres contributes to the observed, relatively high compressive stiffness of the myocardium.

To reflect the stiffening behaviour in the muscle fibre direction, as shown by experimental tests (e.g. figures 2 and 3), it is appropriate to use an exponential function of $I_{4\text{f}}$. Similarly, for the sheet direction, transverse to the muscle fibres; in this direction, the stiffening is in part associated with the collagen fibres connecting the muscle fibres, as discussed above. For this direction, we use an exponential function of the invariant $I_{4\text{s}}$. Clearly, these terms contribute significantly to the stored energy when the associated directions are under tension. However, when they are under compression, their contribution is minimal because the fibres do not support compression. For this reason, we include these terms in

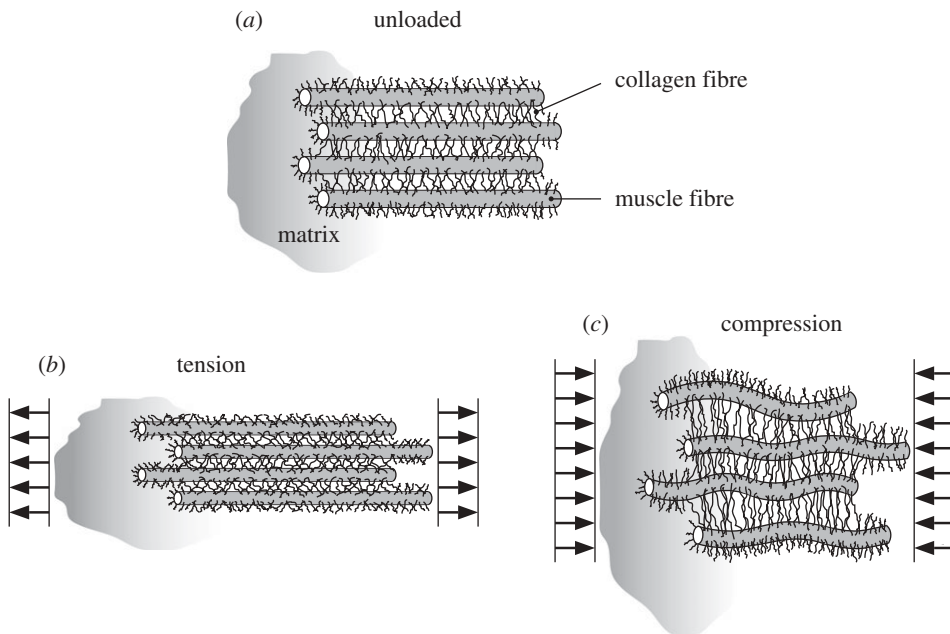


Figure 5. Schematic of the arrangement of muscle and collagen fibres and the surrounding matrix: (a) unloaded structure; (b) structure under tensile load in the muscle fibre direction, showing decreased inter-fibre separation so that the collagen network bears load primarily in the muscle fibre direction; (c) structure under compressive load in the muscle fibre direction, showing the muscle fibres buckled and lateral extension of the collagen network.

the energy function only if $I_{4f} > 1$ or $I_{4s} > 1$, as appropriate. As I_{4n} depends on I_1 , I_{4f} and I_{4s} , we do not include it separately and therefore tensile and compressive behaviour in the normal direction is accommodated by the term in I_1 . These three invariants are sufficient to model the tension/compression behaviour, and there is no need to include I_2 . Indeed, they are also sufficient to characterize the basic features of the shear test results of Dokos *et al.* (2002), which we will demonstrate in the following section.

As far as the more detailed shear behaviour is concerned (figure 2), it is necessary to make use of one or more of the invariants I_{8ij} . In view of the exponential trends shown in figure 2, particularly for the curves (fs) and (fn), we choose to use an exponential function also for this part of the characterization. In particular, as the (nf) and (ns) curves are not distinguished (figure 2), it turns out that we need to consider only the invariant I_{8fs} associated with stretching of the fibres, and not I_{8fn} or I_{8sn} . The above considerations lead us to propose the energy function given by

$$\Psi = \frac{a}{2b} \exp[b(I_1 - 3)] + \sum_{i=f,s} \frac{a_i}{2b_i} \{ \exp[b_i(I_{4i} - 1)^2] - 1 \} + \frac{a_{fs}}{2b_{fs}} [\exp(b_{fs} I_{8fs}^2) - 1], \quad (5.38)$$

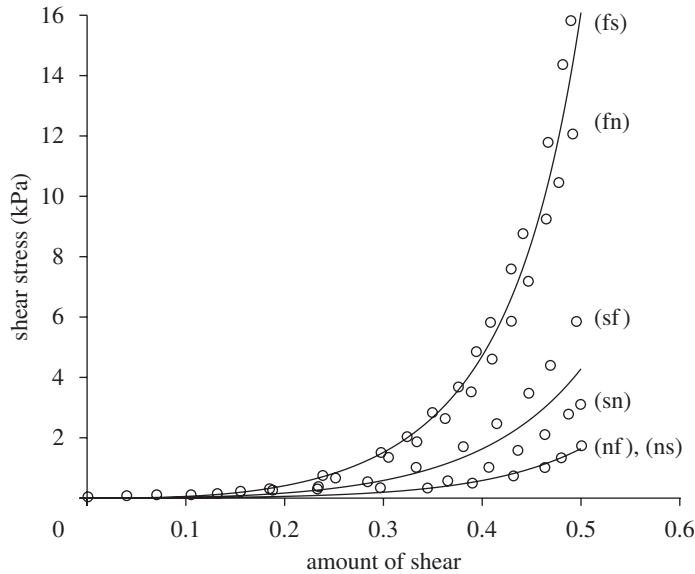


Figure 6. Fit of the model (5.39) with the final term omitted (full curves) to the experimental data (circles) for the loading curves from figure 2: (nf)–(ns) and mean of the loading curves for (fs) and (fn) and for (sf) and (sn). The material parameters used are given in table 1.

where a , b , a_f , a_s , b_f , b_s , a_{fs} and b_{fs} are eight positive material constants, the a parameters having dimension of stress, whereas the b parameters are dimensionless. This consists of the isotropic term in I_1 , the transversely isotropic terms in I_{4f} and I_{4s} and the orthotropic term in I_{8fs} . Note that, if we do not distinguish between the (fs) and (fn) and between the (sf) and (sn) responses, then only six constants are needed.

From equation (5.22), this yields the Cauchy stress

$$\begin{aligned} \boldsymbol{\sigma} = & a \exp[b(I_1 - 3)]\mathbf{B} - p\mathbf{I} + 2a_f(I_{4f} - 1) \exp[b_f(I_{4f} - 1)^2]\mathbf{f} \otimes \mathbf{f} \\ & + 2a_s(I_{4s} - 1) \exp[b_s(I_{4s} - 1)^2]\mathbf{s} \otimes \mathbf{s} + a_{fs}I_{8fs} \exp(b_{fs}I_{8fs}^2)(\mathbf{f} \otimes \mathbf{s} + \mathbf{s} \otimes \mathbf{f}). \end{aligned} \quad (5.39)$$

In the following section, we apply this specific strain-energy function to both biaxial and shear test data and discuss the results in detail.

(d) Fit of the Yin et al. (1987) and Dokos et al. (2002) data

In this section, we show the efficacy of the proposed model for fitting data on the myocardium. First, we use the simplified model based on the three invariants I_1 , I_{4f} and I_{4s} for which the Cauchy stress is given by equation (5.39) with the final term omitted. The resulting fit with the mean of the loading curves for positive (fs) and (fn) and for positive (sf) and (sn) shears, as well as the common curve for positive (nf) and (ns) shears, extracted from figure 2, is shown in figure 6.

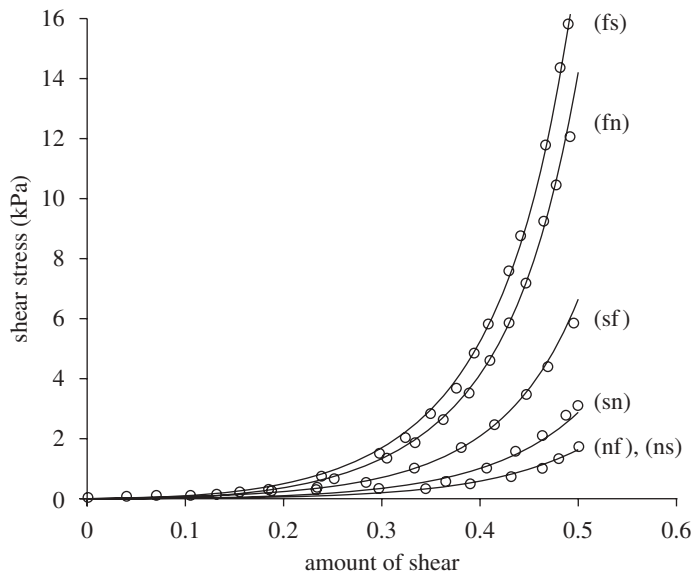


Figure 7. Fit of the model (5.39) (full curves) to the experimental data (circles) for the loading curves from figure 2 with separate (fs), (fn), (sf), (sn) and (nf)–(ns) not distinguished. The material parameters used are given in table 1.

Clearly, this simple model reflects the general characteristics of the distinct shears in the different directions, which exemplify the orthotropy. It is also worth noting that, if the isotropic term is replaced by the neo-Hookean term $\mu(I_1 - 3)/2$, the fit is still relatively good, although the shear stress versus amount of shear is then linear for the (nf)–(ns) plot. We do not show this plot. The data shown in figure 2 indicate that the response for negative shears is very similar to that for positive shear (with reversed sign of the amount of shear and shear stress). Fitting the negative shear data along with those for positive shear would have a minor effect on the values of the fitting parameters.

Second, with this as a starting point, we now refine the fitting by including the final term in equation (5.39), which allows the (fs) and (fn) and the (sf) and (sn) plots to be separated according to figure 2. The resulting fit is shown in figure 7 and indicates very good agreement between the model and the experimental data. As mentioned in §2*b*, we have reversed the labels fn and fs compared with those in Dokos *et al.* (2002). This is because all the other curves in the latter paper show that the (fs) shear response is stiffer than that for (fn). This indeed makes sense because the stiffnesses in the f, s and n directions are, as noted previously, ordered according to $f > s > n$. Thus, the (fs) shear response is expected to be stiffer than the (fn) response. Equally, the (sf) response is stiffer than the (sn) response. It is also suggested that the (nf) response should be stiffer than the (ns) response, although there is no clear distinction seen in figure 2. Other data shown in Dokos *et al.* (2002) do indeed show a small separation in the sense just indicated. The values of the material parameters for the fits shown in figures 6 and 7 are summarized in table 1.

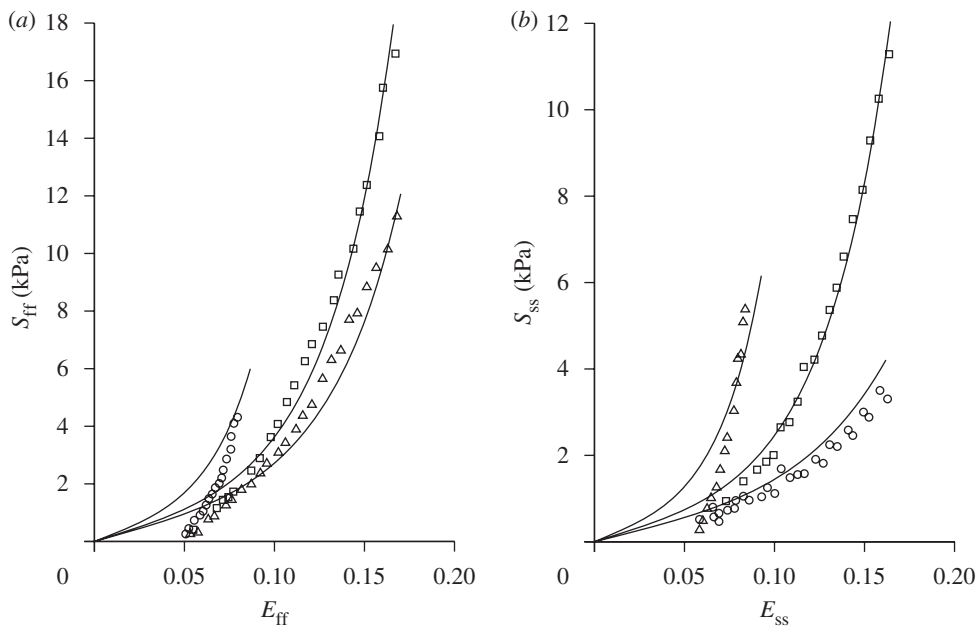


Figure 8. Fit of the model (5.39) to the experimental data of figure 3 (extracted from Yin *et al.* 1987) for three different loading protocols for biaxial loading in the fs plane: (a) stress S_{ff} against strain E_{ff} in the fibre direction; (b) stress S_{ss} against strain E_{ss} in the sheet (cross-fibre) direction. The three sets of experimental data correspond to constant strain ratios E_{ff}/E_{ss} equal to 2.05 (triangles), 1.02 (squares) and 0.48 (circles), whereas the full curves represent the fitted model. The biaxial data can be captured by a transversely isotropic model, and hence only four material constants are required to fit the data. The material parameters used are given in table 1.

Table 1. Material parameters a , b , a_f , b_f , a_s , b_s , a_{fs} and b_{fs} for the energy function (5.38) used to fit the simple shear data for myocardium (Dokos *et al.* 2002) in figures 6 and 7 and the biaxial tension data (Yin *et al.* 1987) in figure 8.

experimental data	a (kPa)	b	a_f (kPa)	b_f	a_s (kPa)	b_s	a_{fs} (kPa)	b_{fs}
shear, figure 6	0.057	8.094	21.503	15.819	6.841	6.959	—	—
shear, figure 7	0.059	8.023	18.472	16.026	2.481	11.120	0.216	11.436
biaxial, figure 8	2.280	9.726	1.685	15.779	—	—	—	—

Next, we use the model (5.39), specialized for the biaxial mode of deformation according to equations (5.36) and (5.37), to fit the experimental data obtained from Yin *et al.* (1987) and shown in figure 8. The associated material parameters are summarized in the last row of table 1.

We are using here the biaxial data of Yin *et al.* (1987) for illustration purposes because, to our knowledge, they are the only true biaxial, as distinct from equibiaxial, data available. However, these data have limitations and, in particular, it should be noted that they do not provide information in the low-strain region (between 0 and 0.05). This highlights the need for more complete

biaxial data. The fit presented in figure 8 is therefore rather crude but can be improved if required by changing the isotropic term, i.e. the I_1 function, and/or by including an activation threshold to accommodate the ‘toe’ region. Whether or not this is done, it is important to recognize that the biaxial data of Yin *et al.* (1987) can be captured by a transversely isotropic specialization of the model. For the model used here, as can be seen from table 1, only four material constants (with $a_s = 0$) are required. Hence, the biaxial data alone appear to suggest that the material is transversely isotropic. As this conflicts sharply with the shear data, care must be taken in drawing conclusions from biaxial data alone. Additional experimental tests are required. For a fuller discussion of the theory underpinning planar biaxial tests for anisotropic nonlinearly elastic solids, we refer to Holzapfel & Ogden (in press).

6. Convexity and related issues

Holzapfel *et al.* (2000) discussed the important issue of convexity of the strain-energy function and its role in ensuring material stability and physically meaningful and unambiguous mechanical behaviour. It is also important for furnishing desirable mathematical features of the governing equations that have, in particular, implications for numerical computation; see also Ogden (2003, 2009) and Holzapfel *et al.* (2004) for further discussion of convexity and related inequalities. For the discussion here, the form of the strain-energy function (5.38) has particular advantages because it is the sum of separate functions of different invariants, with no cross-terms between the invariants involved. This enables the convexity status of each term to be assessed separately. We shall, therefore, consider in succession the three functions $\mathcal{F}(I_1)$, $\mathcal{G}(I_{4f})$ and $\mathcal{H}(I_{8fs})$ as representatives and examine their convexity as a function of the right Cauchy–Green tensor \mathbf{C} .

(a) The function $\mathcal{F}(I_1)$

First we note that

$$\frac{\partial \mathcal{F}(I_1)}{\partial \mathbf{C}} = \mathcal{F}'(I_1) \mathbf{I} \quad \text{and} \quad \frac{\partial^2 \mathcal{F}(I_1)}{\partial \mathbf{C} \partial \mathbf{C}} = \mathcal{F}''(I_1) \mathbf{I} \otimes \mathbf{I}. \quad (6.1)$$

Local convexity of $\mathcal{F}(I_1)$ as a function of \mathbf{C} requires that

$$\frac{\partial^2 \mathcal{F}(I_1)}{\partial \mathbf{C} \partial \mathbf{C}}[\mathbf{A}, \mathbf{A}] \equiv \mathcal{F}''(I_1)(\text{tr } \mathbf{A})^2 \geq 0 \quad (6.2)$$

for all second-order tensors \mathbf{A} , from which we deduce that $\mathcal{F}''(I_1) \geq 0$. Note that strict convexity is not possible because \mathbf{A} can be chosen so that $\text{tr } \mathbf{A} = 0$. For the exponential function considered in equation (5.38), i.e.

$$\mathcal{F}(I_1) = \frac{a}{2b} \{\exp[b(I_1 - 3)] - 1\}, \quad (6.3)$$

this yields $ab \geq 0$. For a non-trivial function, however, we must have $ab > 0$. It is also easy to see that, for the stress response (in simple tension, for example) to be exponentially increasing in the corresponding stretch, we must have $b > 0$. Thus, we have $a > 0$ and $b > 0$.

(b) The function $\mathcal{G}(I_{4f})$

For $\mathcal{G}(I_{4f})$, it follows from the definition of I_{4f} in equation (5.1) that

$$\frac{\partial \mathcal{G}}{\partial \mathbf{C}} = \mathcal{G}'(I_{4f}) \mathbf{f}_0 \otimes \mathbf{f}_0 \quad \text{and} \quad \frac{\partial^2 \mathcal{G}}{\partial \mathbf{C} \partial \mathbf{C}} = \mathcal{G}''(I_{4f}) \mathbf{f}_0 \otimes \mathbf{f}_0 \otimes \mathbf{f}_0 \otimes \mathbf{f}_0. \quad (6.4)$$

Local convexity of $\mathcal{G}(I_{4f})$ requires that

$$\frac{\partial^2 \mathcal{G}}{\partial \mathbf{C} \partial \mathbf{C}} [\mathbf{A}, \mathbf{A}] \equiv \mathcal{G}''(I_{4f}) [(\mathbf{A} \mathbf{f}_0) \cdot \mathbf{f}_0]^2 \geq 0 \quad (6.5)$$

for all second-order tensors \mathbf{A} . It follows that \mathcal{G} is convex in \mathbf{C} provided $\mathcal{G}''(I_{4f}) \geq 0$.

For the exponential form

$$\mathcal{G}(I_{4f}) = \frac{a_f}{2b_f} \{ \exp[b_f(I_{4f} - 1)^2] - 1 \}, \quad (6.6)$$

we obtain

$$\mathcal{G}'(I_{4f}) = a_f(I_{4f} - 1) \exp[b_f(I_{4f} - 1)^2] \quad (6.7)$$

and

$$\mathcal{G}''(I_{4f}) = a_f \exp[b_f(I_{4f} - 1)^2] \{ 1 + 2b_f(I_{4f} - 1)^2 \}. \quad (6.8)$$

For extension in the fibre direction, we have $I_{4f} > 1$, and from equation (6.7) we deduce that for the material response associated with this term to stiffen in the fibre direction we must have $a_f > 0$ and $b_f > 0$. Moreover, these inequalities imply that $\mathcal{G}''(I_{4f}) > 0$ and hence \mathcal{G} is a convex function (both in tension and in compression). It can be shown similarly that the separable Fung-type model (4.7) is convex if the material constants it contains are positive.

As the pole-zero model (4.8) is separable it can be treated on the same basis. For example, if we consider just the first term in equation (4.8), we may write

$$\mathcal{G}(I_{4f}) = \frac{k_{ff} E_{ff}^2}{|a_{ff} - |E_{ff}||^{b_{ff}}}, \quad (6.9)$$

where $I_{4f} = 1 + 2E_{ff}$ and, with $k_{ff} > 0$, $a_{ff} > 0$ and $b_{ff} > 0$, it is straightforward to show that this is convex for all E_{ff} if $0 < b_{ff} \leq 1$ or $b_{ff} \geq 2$. However, it is convex for all E_{ff} such that $|E_{ff}| < a_{ff}$ (which is a necessary restriction) irrespective of the value of $b_{ff} > 0$.

Although the calculations are somewhat different (because the contributions of the different components E_{ij} are not separable), it is also easily shown that the Costa model (4.5) and (4.6) and similar Fung-type models are convex if the coefficients b_{ij} are positive. By contrast, some models are not, in general, convex, as is the case with model (4.2) because of the influence of the term cubic in $\sqrt{I_4} - 1$ and the coupled term in I_1 and I_4 .

(c) The function $\mathcal{H}(I_{8\text{fs}})$

Similar results hold for $\mathcal{H}(I_{8\text{fs}})$. Using the first term in definition (5.3), we calculate

$$\frac{\partial \mathcal{H}}{\partial \mathbf{C}} = \frac{1}{2} \mathcal{H}'(I_{8\text{fs}})(\mathbf{f}_0 \otimes \mathbf{s}_0 + \mathbf{s}_0 \otimes \mathbf{f}_0) \quad (6.10)$$

and

$$\frac{\partial^2 \mathcal{H}}{\partial \mathbf{C} \partial \mathbf{C}} = \frac{1}{4} \mathcal{G}''(I_{8\text{fs}})(\mathbf{f}_0 \otimes \mathbf{s}_0 + \mathbf{s}_0 \otimes \mathbf{f}_0) \otimes (\mathbf{f}_0 \otimes \mathbf{s}_0 + \mathbf{s}_0 \otimes \mathbf{f}_0). \quad (6.11)$$

For an arbitrary second-order tensor \mathbf{A} , we have

$$\frac{\partial^2 \mathcal{H}}{\partial \mathbf{C} \partial \mathbf{C}}[\mathbf{A}, \mathbf{A}] \equiv \mathcal{H}''(I_{8\text{fs}})[(\mathbf{A}\mathbf{f}_0) \cdot \mathbf{s}_0]^2 \quad (6.12)$$

and for convexity this must be non-negative for all \mathbf{A} . Thus, \mathcal{H} is convex in \mathbf{C} provided $\mathcal{H}''(I_{8\text{fs}}) \geq 0$.

For the exponential form

$$\mathcal{H}(I_{8\text{fs}}) = \frac{a_{\text{fs}}}{2b_{\text{fs}}} [\exp(b_{\text{fs}} I_{8\text{fs}}^2) - 1], \quad (6.13)$$

we obtain

$$\mathcal{H}''(I_{8\text{fs}}) = a_{\text{fs}} \exp[b_{\text{fs}}(I_{8\text{fs}} - 1)^2](1 + 2b_{\text{fs}} I_{8\text{fs}}^2), \quad (6.14)$$

so convexity is guaranteed if $a_{\text{fs}} > 0$ and $b_{\text{fs}} > 0$.

In the above discussion based separately on the invariants I_1 , $I_{4\text{f}}$ and $I_{8\text{fs}}$, we have examined only the convexity of individual terms that contribute (additively) to the strain-energy function. If each such term is convex, then the overall strain-energy function is convex. Note, however, that it is not necessary that each such contribution be convex provided any non-convex contribution is counterbalanced by the convexity of the other terms. The analysis of convexity is relatively straightforward for a compressible material, but for an incompressible material more care is needed because then not all components of \mathbf{E} are independent. For discussion of different aspects of convexity, see Holzapfel *et al.* (2000) and Ogden (2003, 2009).

(d) Strong ellipticity and other inequalities

The notion of convexity is different from, but closely related to, aspects of material stability, for discussions of which in the context of the mechanics of soft biological tissues we refer to Holzapfel *et al.* (2004) and Ogden (2003, 2009), for example, and references therein. Whether or not the *strong ellipticity condition* holds is one issue that arises in consideration of material stability. If it holds, then the emergence of certain types of non-smooth deformations, for example, is precluded. For three-dimensional deformations, analysis of the strong ellipticity condition is difficult, especially for anisotropic materials such as those considered here. Necessary and sufficient conditions for strong ellipticity to hold for isotropic materials are available for three dimensions but are very complicated; in two dimensions, they are much more transparent, but their counterparts, even for transversely isotropic materials, are not available. For plane strain deformations, the strong ellipticity condition has been analysed in some detail

by Merodio & Ogden (2002, 2003) for incompressible and compressible fibre-reinforced elastic materials. Here we focus our brief discussion on the anisotropic contributions to the strain-energy function.

If we consider the term $\mathcal{G}(I_{4f})$, for example, on its own, then (Merodio & Ogden 2002) strong ellipticity requires that the inequalities

$$\mathcal{G}'(I_{4f}) + 2I_{4f}\mathcal{G}''(I_{4f}) > 0 \quad \text{and} \quad \mathcal{G}'(I_{4f}) > 0 \quad (6.15)$$

hold. From equation (5.22) and the formula $\mathbf{f} \cdot \mathbf{f} = I_{4f}$, which comes from the first equation in (5.1), it can be seen that the component of Cauchy stress in the fibre direction is given by $2I_{4f}\mathcal{G}'(I_{4f})$. For this to be positive (negative) when $I_{4f} > 1$ (< 1), we require $\mathcal{G}'(I_{4f}) > 0$ (< 0), which means that strong ellipticity does not hold under fibre compression (this is the case for the exponential model; see equation (6.7)). In the context of arterial wall mechanics (Holzapfel *et al.* 2000), this problem is circumvented by recognizing that the fibres tend to buckle in compression and do not support compression to a significant degree, so that the term $\mathcal{G}(I_{4f})$ can be considered to be inactive when $I_{4f} < 1$. Even if this term is not dropped for compression in the fibre direction, its tendency to lead to loss of ellipticity is moderated to some extent by the other terms in the strain-energy function. Turning now to the first inequality in (6.15), we note that this is equivalent to requiring that the nominal stress component in the fibre direction be a monotonic function of the stretch $\sqrt{I_{4f}}$ in that direction, as shown by Merodio & Ogden (2002), which is consistent with the typical stiffening of the stress response of the fibres.

The situation with regard to $\mathcal{H}(I_{8fs})$ is more delicate because, on its own, it can violate strong ellipticity in either tension or compression and generally has a destabilizing influence (Merodio & Ogden 2006). Here we examine its behaviour for simple shear. With reference to equation (5.22), we note that $\mathcal{H}(I_{8fs})$ contributes the term $\mathcal{H}'(I_{8fs})(\mathbf{f} \otimes \mathbf{s} + \mathbf{s} \otimes \mathbf{f})$ to the Cauchy stress $\boldsymbol{\sigma}$. For the simple shear (sf) in the fs plane, we have $\mathbf{f} = \mathbf{f}_0$ and $\mathbf{s} = \gamma\mathbf{f}_0 + \mathbf{s}_0$, where $I_{8fs} = \gamma$ is the amount of shear (see §5*a*(i)). The component of the shear stress on the plane normal to the initial direction \mathbf{s}_0 is then simply $\sigma_{12} = \mathcal{H}'(I_{8fs})$ and we require

$$\mathcal{H}'(\gamma) \gtrless 0 \quad \text{as} \quad \gamma \gtrless 0 \quad (6.16)$$

for the shear stress and strain to be in the same direction. Furthermore, if we require σ_{12} to be a monotonic increasing function of γ , then we must have $\mathcal{H}''(I_{8fs}) \geq 0$, which is consistent with the requirement of convexity in §6*c*.

7. Discussion

To understand the highly nonlinear mechanics of the complex structure of the passive myocardium under different loading regimes, a rationally based continuum model is essential. In the literature to date, models of the myocardium have been mainly of polynomial and/or exponential form, an important exception being the pole-zero model (4.8). Many of the models, including recently published ones, have been based on the assumption of transverse isotropy and are not therefore able to capture the orthotropic response illustrated in the shear data of Dokos *et al.* (2002) on the myocardium. Moreover, not all of these are consistent with convexity requirements noted in §6; an example of such is equation (4.2), as

mentioned in §6. As for the orthotropic models presented in §4*b*, we have already noted the common feature that they are expressed in terms of the components of the Green–Lagrange strain tensor and that these particular components are also expressible in terms of the invariants. Thus, they all fit within the general framework we have outlined in §5. Note, however, that none of them has an explicit isotropic contribution.

Although the Costa *et al.* (2001) model (4.5) and (4.6) has seven material parameters, the model (4.7) has 12 and the pole-zero model in its most general form (4.8) has 18. However, the first of these three models has the disadvantage that the parameters are highly coupled and hence difficult to interpret in terms of the myocardium structure. As pointed out by Schmid *et al.* (2008), the parameter estimation process for the strain-energy function of Costa *et al.* (2001) was reliable, whereas for equation (4.7) and the special case of equation (4.8) with 12 parameters the process was unstable and required more sophisticated strategies, as outlined in their paper. It should be pointed out that, in general, least-squares optimization procedures with large numbers of parameters can lead to non-uniqueness of parameter sets because of sensitivity to small changes in the data (e.g. Fung 1993, §8.6.1). Another common feature is that the orthotropic models reviewed here are somewhat ad hoc in nature and were constructed without the benefit of the general underlying theory such as that described in §5. Nevertheless, in spite of some shortcomings, including lack of convexity in some cases, these models have certainly been helpful in establishing some understanding of the biomechanics of the myocardium.

The specific constitutive model proposed in equation (5.38) has been shown to describe the general characteristics of the available biaxial data relatively well and to fit the available shear data very well. This is a model with only four invariants that is included within the general framework based on six independent invariants for an incompressible orthotropic material, which the myocardium is considered to be. A particular merit of the invariant theory is that it is geometry independent and requires knowledge only of the local preferred directions in the material. Moreover, it is relatively easy to implement within a finite element environment, as is the case with the invariant-based models for arteries (e.g. Holzapfel 2000). The three-dimensional orthotropic model is based on a structural approach in that it takes account of the morphological structure through the muscle fibre direction, the myocyte sheet orientation and the sheet normal direction and considers the resulting macroscopic nature of the myocardium. In this sense, it is not considered to be a micro-mechanically based model. The particular form of the model adopted here uses a set of *eight* material parameters whose interpretations can be based partly on the underlying histology. This number can be reduced to five if the neo-Hookean model is used as the isotropic term for fitting the biaxial data or for illustrating basic features of the different simple shear modes. Construction of the model has been greatly facilitated by the clear structure of the stress–deformation equations that follow from the general form (5.22) and its specializations such as equations (5.23)–(5.28). Furthermore, the model introduced here is consistent with standard inequalities required from considerations of convexity, strong ellipticity and material stability.

Although some aspects of the passive mechanical response of the myocardium seem to be well known, a careful literature survey shows that there are insufficient experimental data available, and there is therefore a pressing need for more

data to inform further development based on the framework discussed in the present work. In terms of the need to simulate the response of the myocardium structure, the next step in our work is to develop a numerical (finite element) realization of the model. Beyond that, with the need for more data emphasized, the constitutive model for the passive behaviour of the myocardium proposed herein may serve as a robust basis for the development of more advanced coupled models that incorporate, for example, active response (muscle contraction), signal transduction and electrophysiology.

The authors thank Thomas Eriksson for his helpful comments on this work and for performing the curve fitting. Financial support for this research was partly provided through an International Joint Project grant from the Royal Society. This support is gratefully acknowledged.

References

- Bischoff, J. E., Arruda, E. M. & Grosh, K. 2002 A microstructurally based orthotropic hyperelastic constitutive law. *J. Appl. Mech.* **69**, 570–579. (doi:10.1115/1.1485754)
- Costa, K. D., Hunter, P. J., Wayne, J. S., Waldman, L. K., Guccione, J. M. & McCulloch, A. D. 1996 A three-dimensional finite element method for large elastic deformations of ventricular myocardium. II. Prolate spheroidal coordinates. *J. Biomech. Eng.* **118**, 464–472. (doi:10.1115/1.2796032)
- Costa, K. D., May-Newman, K., Farr, D., O'Dell, W. G., McCulloch, A. D. & Omens, J. H. 1997 Three-dimensional residual strain in midanterior canine left ventricle. *Am. J. Physiol. Heart Circ. Physiol.* **273**, H1968–H1976.
- Costa, K. D., Holmes, J. W. & McCulloch, A. D. 2001 Modeling cardiac mechanical properties in three dimensions. *Phil. Trans. R. Soc. Lond. A* **359**, 1233–1250. (doi:10.1098/rsta.2001.0828)
- Demer, L. L. & Yin, F. C. P. 1983 Passive biaxial mechanical properties of isolated canine myocardium. *J. Physiol. Lond.* **339**, 615–630.
- Demiray, H. 1972 A note on the elasticity of soft biological tissues. *J. Biomech.* **5**, 309–311. (doi:10.1016/0021-9290(72)90047-4)
- Demiray, H. 1976 Stresses in ventricular wall. *J. Appl. Mech.* **98**, 194–197.
- Dokos, S., Smaill, B. H., Young, A. A. & LeGrice, I. J. 2002 Shear properties of passive ventricular myocardium. *Am. J. Physiol. Heart Circ. Physiol.* **283**, H2650–H2659. (doi:10.1152/ajpheart.00111.2002)
- Frank, J. S. & Langer, G. A. 1974 The myocardial interstitium: its structure and its role in ionic exchange. *J. Cell Biol.* **60**, 586–601. (doi:10.1083/jcb.60.3.586)
- Fung, Y. C. 1993 *Biomechanics: mechanical properties of living tissues*, 2nd edn. New York, NY: Springer.
- Gilbert, S. H., Benson, A. P., Li, P. & Holden, A. V. 2007 Regional localisation of left ventricular sheet structure: integration with current models of cardiac fibre, sheet and band structure. *Eur. J. Cardiothorac. Surg.* **32**, 231–249. (doi:10.1016/j.ejcts.2007.03.032)
- Guccione, J. M., McCulloch, A. D. & Waldman, L. K. 1991 Passive material properties of intact ventricular myocardium determined from a cylindrical model. *J. Biomech. Eng.* **113**, 42–55. (doi:10.1115/1.2894084)
- Holzappel, G. A. 2000 *Nonlinear solid mechanics: a continuum approach for engineering*. Chichester, UK: Wiley.
- Holzappel, G. A. & Ogden, R. W. 2003 *Biomechanics of soft tissue in cardiovascular systems*. CISM Courses and Lectures, no. 441. Wien, NY: Springer.
- Holzappel, G. A. & Ogden, R. W. 2009 *Biomechanical modelling at the molecular, cellular and tissue levels*. CISM Courses and Lectures, no. 508. Wien, Austria: Springer.
- Holzappel, G. A. & Ogden, R. W. In press. On planar biaxial tests for anisotropic nonlinearly elastic solids: a continuum mechanical framework. *Math. Mech. Solids*. (doi:10.1177/1081286507084411)

- Holzapfel, G. A., Gasser, T. C. & Ogden, R. W. 2000 A new constitutive framework for arterial wall mechanics and a comparative study of material models. *J. Elasticity* **61**, 1–48. (doi:10.1023/A:1010835316564)
- Holzapfel, G. A., Gasser, T. C. & Ogden, R. W. 2004 Comparison of a multi-layer structural model for arterial walls with a Fung-type model, and issues of material stability. *J. Biomech. Eng.* **126**, 264–275. (doi:10.1115/1.1695572)
- Horowitz, A., Lanir, Y., Yin, F. C. P., Perl, M., Sheinman, I. & Strumpf, R. K. 1988 Structural three-dimensional constitutive law for the passive myocardium. *J. Biomech. Eng.* **110**, 200–207.
- Humphrey, J. D. & Yin, F. C. P. 1987 On constitutive relations and finite deformations of passive cardiac tissue. Part I. A pseudo-strain energy function. *J. Biomech. Eng.* **109**, 298–304.
- Humphrey, J. D., Strumpf, R. K. & Yin, F. C. P. 1990 Determination of constitutive relation for passive myocardium. I. A new functional form. *J. Biomech. Eng.* **112**, 333–339. (doi:10.1115/1.2891193)
- Hunter, P. J., Nash, M. P. & Sands, G. B. 1997 Computational electromechanics of the heart. In *Computational biology of the heart* (eds A. V. Panfilov & A. V. Holden), pp. 345–407. Chichester, UK: Wiley.
- Huyghe, J. M., van Campen, D. H., Arts, T. & Heethaar, R. M. 1991 The constitutive behaviour of passive heart muscle tissue. A quasi-linear viscoelastic formulation. *J. Biomech.* **24**, 841–849. (doi:10.1016/0021-9290(91)90309-B)
- Huyghe, J. M., Arts, T., van Campen, D. H. & Reneman, R. S. 1992 Porous medium finite element model of the beating left ventricle. *Am. J. Physiol. Heart Circ. Physiol.* **262**, H1256–H1267.
- Katz, L. N. 1977 *Physiology of the heart*. New York, NY: Raven Press.
- Kerckhoffs, R. C. P., Bovendeerd, P. H. M., Kotte, J. C. S., Prinzen, F. W., Smits, K. & Arts, T. 2003 Homogeneity of cardiac contraction despite physiological asynchrony of depolarization: a model study. *Ann. Biomed. Eng.* **31**, 536–547. (doi:10.1114/1.566447)
- LeGrice, I. J., Smaill, B. H., Chai, L. Z., Edgar, S. G., Gavin, J. B. & Hunter, P. J. 1995 Laminar structure of the heart: ventricular myocyte arrangement and connective tissue architecture in the dog. *Am. J. Physiol. Heart Circ. Physiol.* **269**, H571–H582.
- LeGrice, I. J., Hunter, P. J. & Smaill, B. H. 1997 Laminar structure of the heart: a mathematical model. *Am. J. Physiol. Heart Circ. Physiol.* **272**, H2466–H2476.
- MacKenna, D. A., Omens, J. H. & Covell, J. W. 1996 Left ventricular perimysial collagen fibers uncoil rather than stretch during diastolic filling. *Basic Res. Cardiol.* **91**, 111–122. (doi:10.1007/BF00799683)
- Merodio, J. & Ogden, R. W. 2002 Material instabilities in fiber-reinforced nonlinearly elastic solids under plane deformation. *Arch. Mech.* **54**, 525–552.
- Merodio, J. & Ogden, R. W. 2003 Instabilities and loss of ellipticity in fiber-reinforced compressible nonlinearly elastic solids under plane deformation. *Int. J. Solids Structures* **40**, 4707–4727. (doi:10.1016/S0020-7683(03)00309-3)
- Merodio, J. & Ogden, R. W. 2006 The influence of the invariant I_8 on the stress–deformation and ellipticity characteristics of doubly fiber-reinforced non-linearly elastic solids. *Int. J. Non-Linear Mech.* **41**, 556–563. (doi:10.1016/j.ijnonlinmec.2006.02.001)
- Nash, M. P. 1998 Mechanics and material properties of the heart using an anatomically accurate mathematical model. PhD thesis, University of Auckland, Auckland, New Zealand.
- Novak, V. P., Yin, F. C. P. & Humphrey, J. D. 1994 Regional mechanical properties of passive myocardium. *J. Biomech. Eng.* **27**, 403–412. (doi:10.1016/0021-9290(94)90016-7)
- Ogden, R. W. 1997 *Non-linear elastic deformations*. New York, NY: Dover Publications.
- Ogden, R. W. 2003 Nonlinear elasticity, anisotropy and residual stresses in soft tissue. In *Biomechanics of soft tissue in cardiovascular systems* (eds G. A. Holzapfel & R. W. Ogden). CISM Courses and Lectures, no. 441, pp. 65–108. Wien, Austria: Springer.
- Ogden, R. W. 2009 Anisotropy and nonlinear elasticity in arterial wall mechanics. In *Biomechanical modelling at the molecular, cellular and tissue levels* (eds G. A. Holzapfel & R. W. Ogden). CISM Courses and Lectures, no. 508, pp. 179–258. Wien, Austria: Springer.
- Omens, J. H. & Fung, Y. C. 1990 Residual strain in rat left ventricle. *Circ. Res.* **66**, 37–45.
- Rachev, A. 1997 Theoretical study of the effect of stress-dependent remodeling on arterial geometry under hypertensive conditions. *J. Biomech.* **30**, 819–827. (doi:10.1016/S0021-9290(97)00032-8)

- Rodriguez, E. K., Hoger, A. & McCulloch, A. D. 1994 Stress-dependent finite growth in soft elastic tissues. *J. Biomech.* **27**, 455–467. (doi:10.1016/0021-9290(94)90021-3)
- Sands, G. B., Gerneke, D. A., Hooks, D. A., Green, C. R., Smaill, B. H. & LeGrice, I. J. 2005 Automated imaging of extended tissue volumes using confocal microscopy. *Microsc. Res. Tech.* **67**, 227–239. (doi:10.1002/jemt.20200)
- Schmid, H., Nash, M. P., Young, A. A. & Hunter, P. J. 2006 Myocardial material parameter estimation—a comparative study for simple shear. *J. Biomech. Eng.* **128**, 742–750. (doi:10.1115/1.2244576)
- Schmid, H., O’Callaghan, P., Nash, M. P., Lin, W., LeGrice, I. J., Smaill, B. H., Young, A. A. & Hunter, P. J. 2008 Myocardial material parameter estimation: a non-homogeneous finite element study from simple shear tests. *Biomech. Model. Mechanobiol.* **7**, 161–173. (doi:10.1007/s10237-007-0083-0)
- Smaill, B. H. & Hunter, P. J. 1991 Structure and function of the diastolic heart: material properties of passive myocardium. In *Theory of heart: biomechanics, biophysics, and nonlinear dynamics of cardiac function* (eds L. Glass, P. J. Hunter & A. D. McCulloch), pp. 1–29. New York, NY: Springer.
- Spencer, A. J. M. 1984 Constitutive theory for strongly anisotropic solids. In *Continuum theory of the mechanics of fibre-reinforced composites* (ed. A. J. M. Spencer). CISM Courses and Lectures, no. 282, pp. 1–32. Wien, Austria: Springer.
- Vossoughi, J., Vaishnav, R. N. & Patel, D. J. 1980 Compressibility of the myocardial tissue. In *Advances in bioengineering* (ed. Van C. Mow), pp. 45–48. New York, NY: Bioengineering Division, American Society of Mechanical Engineers.
- Yin, F. C. P. 1981 Ventricular wall stress. *Circ. Res.* **49**, 829–842.
- Yin, F. C. P., Strumpf, R. K., Chew, P. H. & Zeger, S. L. 1987 Quantification of the mechanical properties of noncontracting canine myocardium under simultaneous biaxial loading. *J. Biomech.* **20**, 577–589. (doi:10.1016/0021-9290(87)90279-X)
- Young, A. A., LeGrice, I. J., Young, M. A. & Smaill, B. H. 1998 Extended confocal microscopy of myocardial laminae and collagen network. *J. Microsc.* **192**, 139–150. (doi:10.1046/j.1365-2818.1998.00414.x)